

**IMAGE PROCESSING WITH THE FRACTIONAL
FOURIER TRANSFORM: SYNTHESIS,
COMPRESSION AND PERSPECTIVE PROJECTIONS**

A THESIS

**SUBMITTED TO THE DEPARTMENT OF ELECTRICAL
AND ELECTRONICS ENGINEERING
AND THE INSTITUTE OF ENGINEERING AND SCIENCES
OF BILKENT UNIVERSITY
IN PARTIAL FULFILLMENT OF THE REQUIREMENTS
FOR THE DEGREE OF
MASTER OF SCIENCE**

By

I. Şamil Yetik

August 2000

THESIS
QA
403.5
.Y48
2000

IMAGE PROCESSING WITH THE FRACTIONAL
FOURIER TRANSFORM: SYNTHESIS,
COMPRESSION AND PERSPECTIVE PROJECTIONS

A THESIS

SUBMITTED TO THE DEPARTMENT OF ELECTRICAL
AND ELECTRONICS ENGINEERING
AND THE INSTITUTE OF ENGINEERING AND SCIENCES
OF BILKENT UNIVERSITY
IN PARTIAL FULFILLMENT OF THE REQUIREMENTS
FOR THE DEGREE OF
MASTER OF SCIENCE

By

İ. Şamil Yetik
August 2000

QA

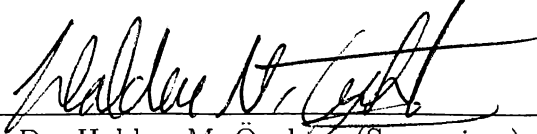
403.5

'748

2000

B053048

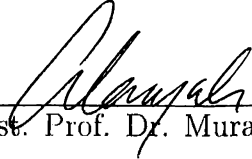
I certify that I have read this thesis and that in my opinion it is fully adequate,
in scope and in quality, as a thesis for the degree of Master of Science.


Prof. Dr. Haldun M. Özaktas (Supervisor)

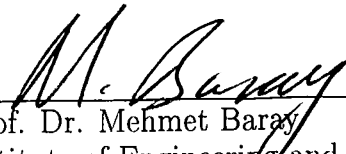
I certify that I have read this thesis and that in my opinion it is fully adequate,
in scope and in quality, as a thesis for the degree of Master of Science.


Prof. Dr. A. Enis Çetin

I certify that I have read this thesis and that in my opinion it is fully adequate,
in scope and in quality, as a thesis for the degree of Master of Science.


Assist. Prof. Dr. Murat Alanyalı

Approved for the Institute of Engineering and Sciences:


Prof. Dr. Mehmet Baray
Director of Institute of Engineering and Sciences

ABSTRACT

SIGNAL PROCESSING APPLICATIONS OF THE FRACTIONAL FOURIER TRANSFORM

İ. Şamil Yetik

M. S. in Electrical and Electronics Engineering

Supervisor: Prof. Dr. Haldun M. Özaktaş

August 2000

In this work, first we give a summary of the fractional Fourier transform including its definition, important properties, generalization to two-dimensions and its discrete counterpart. After that, we repeat the concept of filtering in the fractional Fourier domains and give multi-stage and multi-channel filtering configurations. Due to the nonlinear nature of the problem, the transform orders in fractional Fourier domain filtering configurations have usually not been optimized but chosen uniformly up to date. We discuss the optimization of orders in the multi-channel filtering configuration. In the next part of this thesis, we discuss the application of fractional Fourier transform based filtering configurations to image representation and compression. Next, we introduce the fractional Fourier domain decomposition for continuous signals and systems. In the last part, we analyse perspective projections in the space-frequency plane and show that under certain conditions they can be approximately modeled in terms of the fractional Fourier transform.

Keywords: Fractional Fourier transforms, signal and system synthesis, image representation and compression, perspective projections.

ÖZET

KESİRLİ FOURIER DÖNÜŞÜMÜNÜN SİNYAL İŞLEME UYGULAMALARI

İ. Şamil Yetik

Elektrik ve Elektronik Mühendisliği Bölümü Yüksek Lisans

Tez yöneticisi: Prof. Dr. Haldun M. Özaktaş

Ağustos 2000

Bu çalışmada, önce kesirli Fourier dönüşümünün bir özeti verildi. Bu özetde, kesirli Fourier dönüşümünün tanımı, önemli özellikleri, iki boyuta genellenmesi ve sayısal kesirli Fourier dönüşümünün tanımı verildi. Daha sonra, kesirli Fourier domenlerinde süzgeçleme ve çok kanallı ve çok kademeli süzgeçleme düzenekleri tanımlandı. Bu düzeneklerde doğrusal olmayan bir yapı gözleendiğinden, bu zamana kadar dönüşüm dereceleri düzgün dağılımlı olarak alınmıştı. Bu çalışmada, bu dereceler üzerinden iyileştirmeyi sağlayan bir yöntem sunuldu. Bir sonraki bölümde, kesirli Fourier dönüşümü süzgeçleme düzeneklerinin görüntü sıkıştırılması alanında kullanımı gösterildi. Daha sonra, devamlı işaretler için kesirli Fourier domen çözümlemesi tanımlandı. Son olarak, perspektif izdüşüm uzay-sıklık düzleminde incelenerek, perspektif izdüşüm ile kesirli Fourier dönüşümü arasındaki ilişki irdelendi. Belli şartlar altında, kesirli Fourier dönüşümü kullanılarak, perspektif izdüşümünü yaklaşık olarak elde etmenin bir yöntemi verildi.

Anahtar Kelimeler: kesirli Fourier dönüşümü, işaret ve sistem sentezi, görüntü sıkıştırılması, perspektif izdüşüm.

ACKNOWLEDGMENTS

I would like to express my deepest gratitude to Prof. Dr. Haldun M. Özaktas for his excellent supervision, guidance, suggestions and endless patience.

I would also like to thank the members of my committee, Prof. Dr. A. Enis Çetin and Assist. Prof. Dr. Murat Alanyalı for their comments on the thesis.

Finally and mostly, I want to express my sincere and deepest thanks to my family for their endless support throughout my education.

Contents

1	Introduction	1
2	The Fractional Fourier Transform	5
2.1	Introduction and History	5
2.2	Definition and Properties	7
3	Optimization of Orders in Multi-Channel Fractional Fourier Domain Filtering Configurations	12
3.1	Filtering Configurations Based on the Fractional Fourier Transform	12
3.2	Optimization of Orders in the Multi-Channel Filtering Configuration	15
4	Image Representation and Compression with the Fractional Fourier Transform	23
5	Continuous Fractional Fourier Domain Decomposition	27
6	Perspective Projections and Fractional Fourier Transforms	29
6.1	Introduction	29
6.2	Perspective Projections	30
6.3	Perspective Projections and Fractional Fourier Transforms	33
6.4	Error Analysis	41
7	Conclusions and Future Work	47

List of Figures

2.1	The fractional Fourier transforms of a rect with a continuum of orders	9
3.1	Fractional Fourier transform based filtering configurations	14
3.2	Gaussian Schell-model mutual intensity synthesis	19
3.3	Rectangular mutual intensity synthesis	21
4.1	Image compression example	26
6.1	Perspective model	31
6.2	Wigner distribution of an exponential and a chirp	33
6.3	Illustration of the decomposition of the approximation into elementary operations in the space-frequency plane	35
6.4	Perspective projection approximation: example 1	37
6.5	Perspective projection approximation: example 2	38
6.6	2D Perspective model	39
6.7	2D Perspective projection approximation: example	42
6.8	Comparison of Wigner distributions underlying error analysis . . .	44
6.9	Valid regions of the perspective projection approximation	45

Chapter 1

Introduction

Digital signal processing has found a central place in signal processing after the popular use of digital computers in various applications, where one needs to process signals for many purposes like transmitting, storing, compressing, enhancement and many others. Some of the systems of the processes mentioned above are non-linear, some of them are linear. However, linear systems are easy to handle and in some applications they constitute a group of systems that is adequate for many purposes. Linear systems can also be used to model non-linear systems. Because of these reasons, linear systems have been extensively emphasized in digital signal processing.

A general linear system can be characterized as,

$$g(u) = \int H(u, u') f(u') du', \quad (1.1)$$

where $H(u, u')$ is called the kernel of the system and $g(u)$ and $f(u)$ are the output and input of the system, respectively. Discrete version of 1.1 can be expressed as,

$$g[n] = \sum_{k=0}^{N-1} H[n, k] f[k], \quad (1.2)$$

where $g[n]$ and $f[n]$ are either samples of $f(u)$ and $g(u)$ or discrete functions that somehow occur in digital systems, and $H[n, k]$ are either samples of $H(u, u')$

or the kernel of a digital system. The last equation is simply a matrix vector multiplication which can also be written as,

$$\mathbf{g} = \mathbf{H}\mathbf{f}, \quad (1.3)$$

where \mathbf{g} and \mathbf{f} are vectors representing $g[n]$ and $f[n]$ and \mathbf{H} is a matrix representing $H[n, k]$. A detailed discussion of the signals and systems may be found in [1, 2].

In many applications, we face with linear systems that are shift-invariant. In the case of shift-invariant systems, when the input is shifted by a certain amount, the output is also shifted by the same amount. This property is equivalent to having a kernel of the special form $H(u, u') = h(u - u')$. Fourier transform is a very powerful tool in analyzing shift-invariant systems, because shift-invariant systems correspond to a multiplication in the Fourier domain. Turning our attention to the digital case, matrices representing the shift-invariant digital systems are circulant matrices and the Fourier transform matrix (DFT) diagonalizes the kernel matrix. There exists a fast algorithm (FFT) that allows us to compute Fourier transform in $O(N \log N)$ time (Here N is the length of the discrete signal vectors or the time/space-bandwidth product of continuous signals). This efficient implementation is the main reason that Fourier transform plays a central role in the analysis of shift-invariant systems.

We can think of the general linear systems and shift-invariant linear systems as the two extremes. In one end, implementation cost is $O(N \log N)$ (shift-invariant systems), and in the other end, implementation cost is $O(N^2)$ (general linear systems). In some applications, shift-invariant systems may be inadequate but efficient, and general linear systems may be adequate but inefficient. This situation suggests to search for a way to be able to trade-off between cost and performance. One way which makes this trade-off possible is the use of fractional Fourier transform. The fractional Fourier transform is a generalization of the ordinary Fourier transform; definition and some of its properties will be given in

the next chapter.

The original contribution of this thesis to the research area is summarized in this part. The optimization of orders in fractional Fourier transform has not been addressed before, in this thesis we have given a method to optimize orders in the multi-channel filtering configuration. Although fractional Fourier transform based filtering configurations are used in system/signal synthesis, signal restoration and feature extraction, the idea of using fractional Fourier transform based filtering configurations in image representation and compression is introduced in this thesis, for the first time. Continuous counterpart of fractional Fourier domain decomposition is defined. Finally, relation between perspective projections and fractional Fourier transforms are also studied in detail, and it is shown that perspective projections can be approximated by fractional Fourier transforms under certain conditions.

In Chapter 2, we give the definition of the fractional Fourier transform and some of its important properties. Also, we are going to give a brief history of the fractional Fourier transform and mention some of the applications where the fractional Fourier transform is used. In Chapter 3, we give the concept of filtering in fractional Fourier domains and represent the multi-stage and multi-channel filtering configurations. Also, we discuss the optimization of fractional Fourier transform orders for multi-channel filtering configurations by first finding the optimal filter coefficients for a larger number of uniformly chosen orders, and then maintaining the most important ones. Chapter 4 is reserved for the discussion of the application of fractional Fourier transform based filtering configurations to image representation and compression. In Chapter 5, we define continuous version of fractional Fourier domain decomposition, of which the discrete version and its applications were studied before.

In Chapter 6, we analyse perspective projections in the space-frequency plane and show that under certain conditions they can be approximately modeled in terms of the fractional Fourier transform. Conclusions and future work are discussed in Chapter 7.

Chapter 2

The Fractional Fourier Transform

2.1 Introduction and History

The fractional Fourier transform is a one-parameter generalization of the ordinary Fourier transform. We obtain the fractional Fourier transform by using this parameter as the functional power of the ordinary Fourier transform.

The fractional Fourier transform is introduced to the mathematics community by the early papers [3-5]. However, it did not draw much attention until it has been used by optics and signal processing communities. Number of publications has exploded after 1980's when it has found its place in optics and signal processing.

The fractional Fourier transform suggests a potential improvement in the applications where ordinary Fourier transform is used, since it provides an extra parameter. We can improve the solution to any problem that had previously utilized Fourier transform, by carrying the extra parameter throughout the solution and then optimizing over this parameter. We can group the several applications of the fractional Fourier transform as: i) applications in mathematics and physics, ii) optical information processing applications and iii) digital signal processing applications.

In this thesis, we are more interested in signal processing applications of the fractional Fourier transform, however we briefly give some selected publications in other areas as well. Mathematics and physics applications of the fractional Fourier transform [6–8] include quantum mechanics, uncertainty principles and solution to differential equations. Optics applications of the fractional Fourier transform [9–16] include optical propagation and diffraction, analysis and design of Fourier optical systems, beam shaping and other applications.

Fractional Fourier domains are first introduced in [17], and many applications of the fractional Fourier transform has been based on this concept. Optimum Wiener filtering in fractional Fourier domains are studied in [18]. In this paper, analytic solutions are presented that yield the optimum fractional Fourier domain and optimum filter coefficients corresponding to this domain. As an application of the optimal filtering in fractional Fourier domains, optimal image restoration is studied in [19]. In these papers, a single fractional Fourier domain has been used. The concept of generalizing the fractional Fourier domain filtering to two or more number of domains has been studied in two directions mostly. First one is multi-stage filtering, which is defined as filtering in consecutive fractional Fourier domains, and has been studied in [20]. Multi-stage filtering has found applications in signal restoration [20], system synthesis [21], mutual intensity synthesis [22]. Second one is multi-channel filtering, which is defined as filtering in parallel fractional Fourier domains in [23]. Multi-channel filtering has been used in system decomposition [24,25]. In [24], fractional Fourier domain decomposition is defined and its applications like efficient implementations of linear systems are given. Other applications of multi-channel filtering including signal recovery and restoration, signal synthesis and system synthesis has been studied in [23]. Continuous version of fractional Fourier domain decomposition is defined in [25]. The fractional correlation is first defined in [26] and developed in [27]. The concept of fractional correlation is used in pattern recognition in [28, 29]. Also, feature extraction using the fractional Fourier transform can be found in [30].

Some of the other references related to the fractional Fourier transform and its applications can be listed as [31–41].

Here, we do not give the complete list of references, for a more complete list one can refer to [2].

2.2 Definition and Properties

The a th order fractional Fourier transform of the function $f(u)$ will be denoted by $f_a(u)$. Here, we are going to give the linear system kernel definition of the fractional Fourier transform. Other equivalent definitions can be found in [2]. The fractional Fourier transform of a signal is defined as:

$$f_a(u) = \int K_a(u, u') f(u') du', \quad (2.1)$$

$$K_a(u, u') = A_\phi \exp \left[i\pi (\cot \phi u^2 - 2 \csc \phi uu' + \cot \phi u'^2) \right],$$

where

$$\phi = \frac{a\pi}{2}, \quad (2.2)$$

$$A_\phi = \sqrt{1 - i \cot \phi}. \quad (2.3)$$

The square root is defined such that the argument of the result lies in the interval $(-\pi/2, \pi/2]$. When a is an even integer the above kernel is undefined. However, it is possible to show that as a approaches an even integer, the kernel approaches a delta function. That is, $K_{4j}(u, u') = \delta(u - u')$ and $K_{4j\pm 2}(u, u') = \delta(u + u')$, where j is an arbitrary integer.

Now, we are going to give some special cases of the fractional Fourier transform. The fractional Fourier transform is equal to the identity operation when $a = 0$, to the ordinary Fourier transform when $a = 1$, to the parity operation when $a = 2$ and to the inverse Fourier transform when $a = 3$. Close examination of the kernel given in 2.1 reveals that the fractional Fourier transform is periodic in a with period 4. The fractional Fourier transform interpolates between the 0th

order fractional Fourier transform (original function) and the 1st order fractional Fourier transform (ordinary Fourier transform of the signal). This is illustrated for a rect function in Figure 2.1.

Having given the definition, now we are going to have a look at the important properties of the fractional Fourier transform, briefly. First, the fractional Fourier transform is a one parameter generalization of the ordinary Fourier transform and it is a member of the linear canonical transforms. Another important property of the fractional Fourier transform is index additivity. That is, a_1 th order fractional Fourier transform of the a_2 th order fractional Fourier transform is equal to the $(a_1 + a_2)$ th order fractional Fourier transform. Relation between the fractional Fourier transform and the Wigner distribution is of central importance in many applications. Before giving this relation, we are going to give the definition and some important properties of the Wigner distribution here for convenience.

The Wigner distribution $W_f(u, \mu)$ of a function $f(u)$ is defined as

$$W_f(u, \mu) = \int f(u + u'/2) f^*(u - u'/2) e^{-2\pi i \mu u'} du', \quad (2.4)$$

where μ represents the Fourier domain variable. $W_f(u, \mu)$ can also be expressed in terms of $F(\mu)$ (the Fourier transform of $f(u)$), or indeed as a function of any fractional Fourier transform of $f(u)$. Some of its most important properties are:

$$|f(u)|^2 = \int W_f(u, \mu) d\mu, \quad (2.5)$$

$$|F(\mu)|^2 = \int W_f(u, \mu) du, \quad (2.6)$$

$$\text{En}[f(u)] = \int W_f(u, \mu) du d\mu, \quad (2.7)$$

$\text{En}[f(u)]$ is the total energy of the signal $f(u)$. These properties reveal that Wigner distribution gives the distribution of the signal energy over space and frequency. The Wigner distribution of $F(\mu)$, is a ninety degree rotated version of the Wigner distribution of $f(u)$. More on the Wigner distribution and other such distributions and representations may be found in [42].

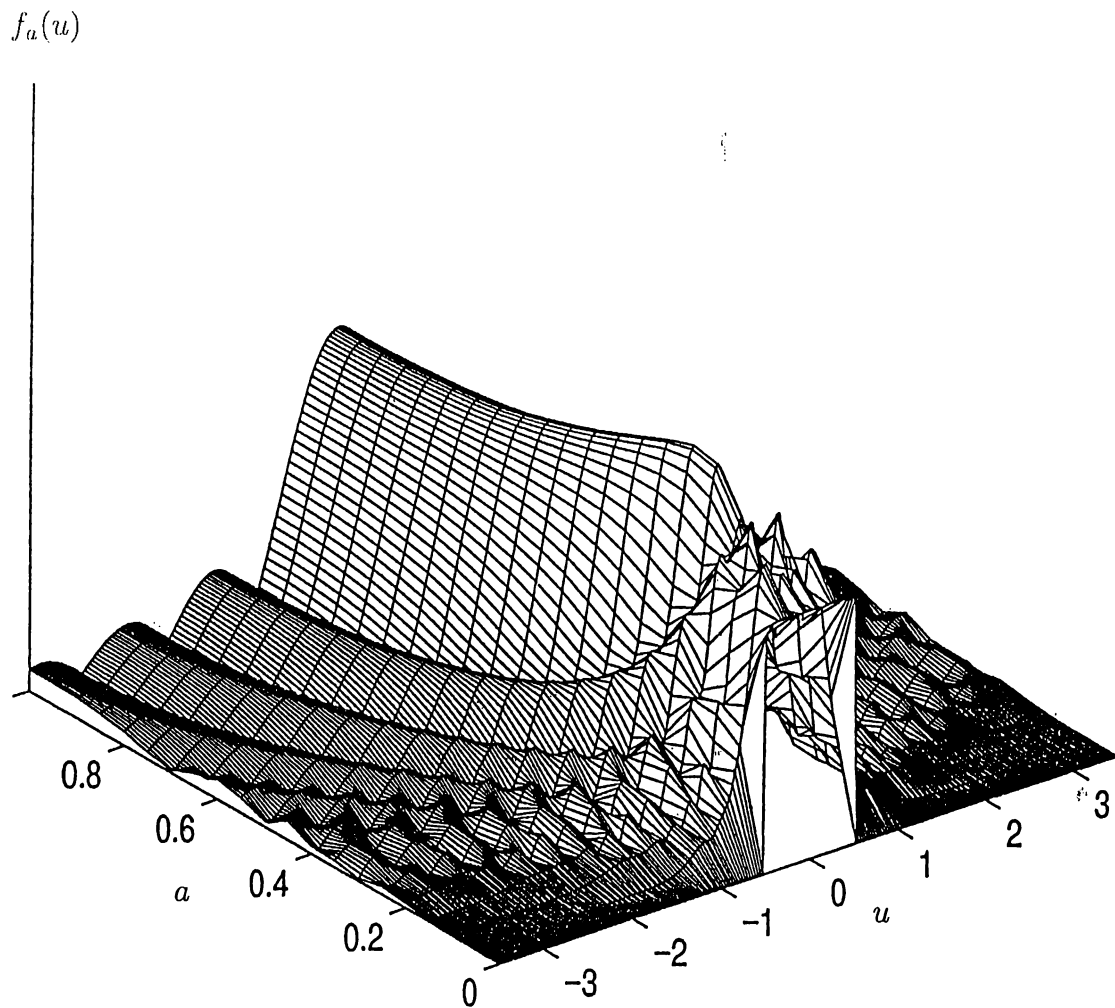


Figure 2.1: Axis ranging from 0 to 1 indicates the fractional Fourier transform order. Each slices of this three-dimensional figure corresponds to the fractional Fourier transform of the rect function with a certain order. When $a = 1$, we observe the Fourier transform of the rect: a sinc (After [48]).

If $W_f(u, \mu)$ denotes the Wigner distribution of $f(u)$, then the Wigner distribution of the a th order fractional Fourier transform of $f(u)$, denoted by $W_{f_a}(u, \mu)$, is given by:

$$W_{f_a}(u, \mu) = W_f(u \cos \phi - \mu \sin \phi, u \sin \phi + \mu \cos \phi), \quad (2.8)$$

that is, the Wigner distribution of $f_a(u)$ is the clockwise rotated version of the Wigner distribution of $f(u)$ by an angle ϕ . A result of this property is as follows:

$$\int W_{f_a}(u, \mu) d\mu = |f_a(u)|^2. \quad (2.9)$$

That is, the integral projection of the Wigner distribution of a function onto the u_a axis is equal to the magnitude square of the a th order fractional Fourier transform of the function.

Finally, there exists a fast implementation of the fractional Fourier transform [43] with implementation cost $O(N \log(N))$. Actually, this fast implementation makes it possible to use the fractional Fourier transform in applications where the ordinary Fourier transform is used, with no additional cost, resulting in possible improvements. However we should note that, this fast implementation cannot be interpreted as the discrete fractional Fourier transform, because it does not satisfy important properties like index additivity and Wigner rotation property, exactly.

Discrete fractional Fourier transform is defined in [44]. The discrete fractional Fourier transform satisfies the properties of the continuous fractional Fourier transform. But, an efficient implementation of the discrete fractional Fourier transform has not been found up to this date.

Until now, we have considered only the one-dimensional definition of the fractional Fourier transformation. Here, we will generalize the definition of the fractional Fourier transform to two-dimensions. There are two ways of generalizing the definition to two-dimensional systems.

First one is the separable two-dimensional fractional Fourier transform defined as:

$$\begin{aligned} f_{\mathbf{a}}(\mathbf{q}) &= f_{a_u, a_v}(u, v) = \mathcal{F}^{\mathbf{a}} f(\mathbf{q}) = \mathcal{F}^{a_u, a_v} f(u, v) \\ &= \int \int K_{a_u, a_v}(u, v; u', v') f(u', v') du' dv', \\ K_{a_u, a_v}(u, v; u', v') &= K_{a_u}(u, u') K_{a_v}(v, v'), \end{aligned} \quad (2.10)$$

for two dimensions and similarly for higher dimensions. Here $\mathbf{q} = u\hat{\mathbf{u}} + v\hat{\mathbf{v}}$ and $\mathbf{a} = a_u\hat{\mathbf{u}} + a_v\hat{\mathbf{v}}$ where $\hat{\mathbf{u}}$ and $\hat{\mathbf{v}}$ are unit vectors in the u and v directions. $K_a(u, u')$ is the one-dimensional kernel defined in equation 2.1.

Second one is the non-separable two-dimensional fractional Fourier transform defined as /citetwod:

$$\mathcal{F}_{\theta_1, \theta_2}^{a_u, a_v} \{f(\mathbf{q})\} = \int_{-\infty}^{\infty} B_{\theta_1, \theta_2}^{a_u, a_v}(\mathbf{q}, \mathbf{q}'') f(\mathbf{q}'') d\mathbf{q}'', \quad (2.11)$$

where

$$B_{\theta_1, \theta_2}^{a_u, a_v}(\mathbf{q}, \mathbf{q}'') = K_q \exp[i\pi(\mathbf{q}^T \mathbf{A} \mathbf{q} + 2\mathbf{q}^T \mathbf{B} \mathbf{q}'' + \mathbf{q}''^T \mathbf{C} \mathbf{q}'')] \quad (2.12)$$

with

$$K_q = K_{u'} K_{v'}, \quad \mathbf{r} = \begin{bmatrix} u & v \end{bmatrix}^T, \quad \mathbf{q}'' = \begin{bmatrix} u'' & v'' \end{bmatrix}^T,$$

$$\mathbf{A} = \begin{bmatrix} \cot \phi_{u'} & 0 \\ 0 & \cot \phi_{v'} \end{bmatrix},$$

$$\mathbf{B} = \begin{bmatrix} -\frac{\cos \theta_2 \csc \phi_{u'}}{\cos(\theta_1 - \theta_2)} & \frac{\sin \theta_1 \csc \phi_{u'}}{\cos(\theta_1 - \theta_2)} \\ -\frac{\sin \theta_2 \csc \phi_{v'}}{\cos(\theta_1 - \theta_2)} & -\frac{\cos \theta_1 \csc \phi_{v'}}{\cos(\theta_1 - \theta_2)} \end{bmatrix},$$

$$\mathbf{C} = \begin{bmatrix} \frac{\cos^2 \theta_2}{\cos^2(\theta_1 - \theta_2)} \cot \phi_{u'} + \frac{\sin^2 \theta_2}{\cos^2(\theta_1 - \theta_2)} \cot \phi_{v'} & -\frac{\sin \theta_1 \cos \theta_2}{\cos^2(\theta_1 - \theta_2)} \cot \phi_{u'} + \frac{\sin \theta_2 \cos \theta_1}{\cos^2(\theta_1 - \theta_2)} \cot \phi_{v'} \\ -\frac{\sin \theta_1 \cos \theta_2}{\cos^2(\theta_1 - \theta_2)} \cot \phi_{u'} + \frac{\sin \theta_2 \cos \theta_1}{\cos^2(\theta_1 - \theta_2)} \cot \phi_{v'} & \frac{\cos^2 \theta_1}{\cos^2(\theta_1 - \theta_2)} \cot \phi_{v'} + \frac{\sin^2 \theta_1}{\cos^2(\theta_1 - \theta_2)} \cot \phi_{u'} \end{bmatrix}.$$

Here we give the definitions of the fractional Fourier transform for the sake of completeness. These two-dimensional fractional Fourier transforms will not be employed in this thesis.

Chapter 3

Optimization of Orders in Multi-Channel Fractional Fourier Domain Filtering Configurations

3.1 Filtering Configurations Based on the Fractional Fourier Transform

Space- and frequency-domain filtering are special cases of fractional Fourier domain filtering (3.1(a,b,c)) [18, 46]. Fractional Fourier domain filtering consists of (i) taking the fractional Fourier transform of the input signal, (ii) multiplication with a filter function, and (iii) taking the inverse fractional Fourier transform of the result. The fractional version of the optimal Wiener filtering problem has been studied in detail in [18]. Fractional Fourier domain filtering has been further generalized to multi-stage and multi-channel filtering (3.1(e,f)). In multi-stage filtering [21, 47] the input is first transformed into the a_1 th domain, where it is multiplied by a filter h_1 . The result is then transformed back into the original domain. This process is repeated M times. Denoting the diagonal matrix

corresponding to multiplication by the k th filter by Λ_k , we can write the following expression for the overall effect of the multi-stage filtering configuration:

$$\mathbf{T}_{\text{ms}} = \left[\mathbf{F}^{-a_M} \Lambda_{h_M} \dots \mathbf{F}^{a_2 - a_1} \Lambda_{h_1} \mathbf{F}^{a_1} \right], \quad (3.1)$$

where \mathbf{T}_{ms} is a matrix representing the overall multi-stage filtering configuration and \mathbf{F}^{a_k} denotes the discrete fractional Fourier transform matrix [44]. Multi-channel filtering configurations [24,47] consist of M single-stage blocks in parallel. For each channel k , the input is transformed to the a_k th domain, multiplied by a filter h_k and then transformed back. Now, we can write the following expression for the overall effect of the multi-channel filtering configuration:

$$\mathbf{T}_{\text{mc}} = \left[\sum_{k=1}^M \mathbf{F}^{-a_k} \Lambda_k \mathbf{F}^{a_k} \right] \quad (3.2)$$

where \mathbf{T}_{mc} is a matrix representing the overall multi-channel filtering configuration. It is possible to further generalize these filtering configurations by using parallel and series arrangements together; such systems have been called generalized filtering circuits [47, 48]. The problem of finding the optimal filter coefficients, given the transform orders, has been solved in [18, 21, 47]. Given a matrix \mathbf{H} which represents a system one wishes to synthesize, one seeks the filter coefficients such that the resulting matrices \mathbf{T}_{ms} or \mathbf{T}_{mc} is as close as possible to \mathbf{H} according to some specified criteria, such as mean square error. Until now, the transform orders have usually been chosen uniformly ($a_1 = 1/M, a_2 = 2/M, \dots, a_M = 1$); the problem of optimizing the orders has not yet been addressed. In this chapter, we show how one can optimize over the orders

A A A for multi-channel filtering by first finding the optimal filter coefficients for a larger number of uniformly chosen orders, and then maintaining the most important ones.

In [21, 24, 47] fractional Fourier transform based filtering configurations have been used for approximating linear space-variant systems, represented by some

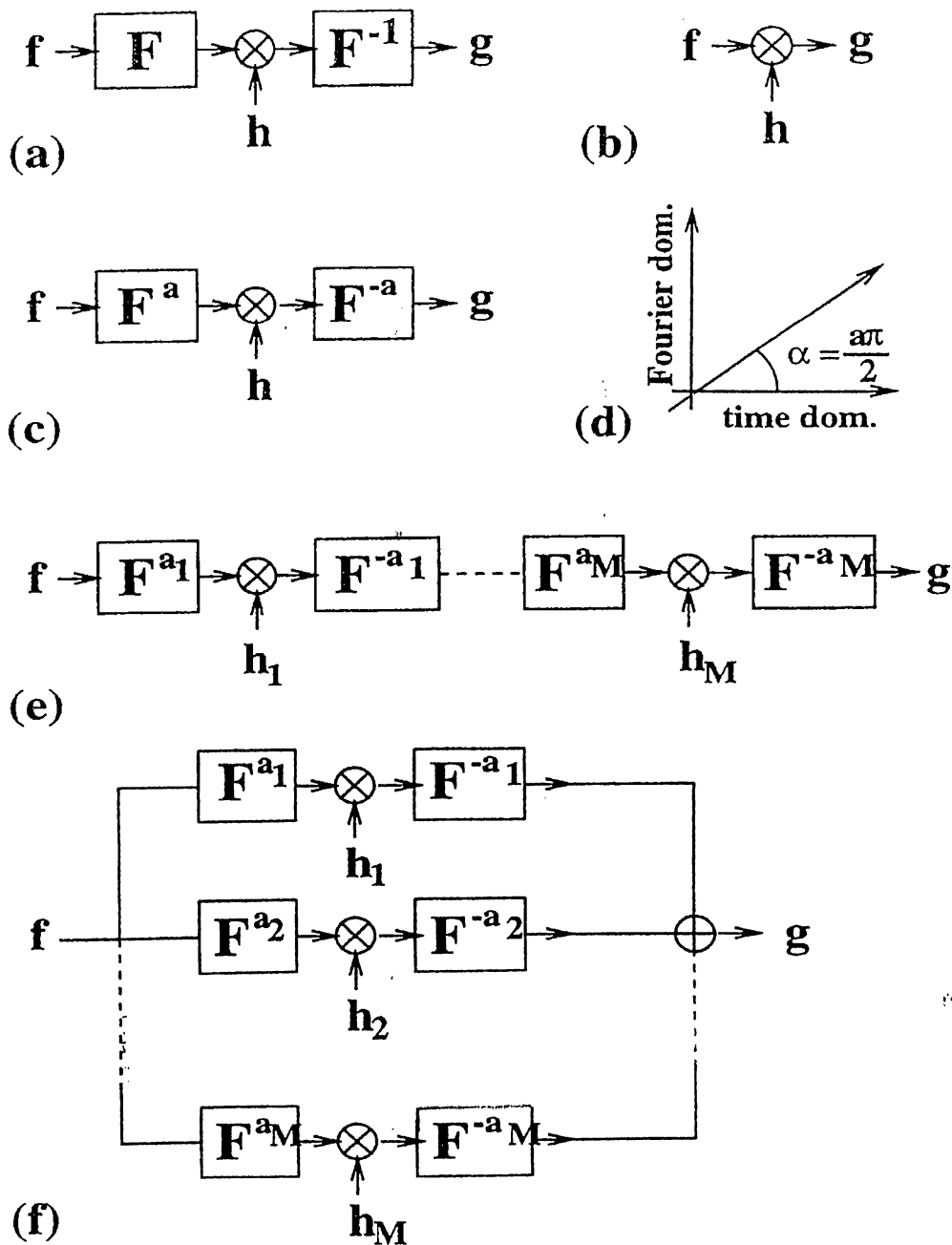


Figure 3.1: a) Fourier domain filtering. b) Space domain filtering. c) a th order fractional Fourier domain filtering. d) a th order fractional Fourier domain. e) Multi-stage filtering. f) Multi-channel filtering. (After [22])

matrix \mathbf{H} . It was shown that for many such systems encountered in various applications, it is possible to approximate the system \mathbf{H} with a multi-stage or multi-channel configuration \mathbf{T}_{ms} or \mathbf{T}_{mc} with acceptable mean square error, by using a small or moderate number (M) of stages or channels. Since the cost of implementing the fractional Fourier transform (optically or digitally) is similar to the cost of implementing the ordinary Fourier transform, this leads to a fast implementation of the space-variant system in question. For instance, for digital systems, the cost becomes $O(MN \log N)$, which should be compared to the cost $O(N^2)$ for direct implementation of linear systems.

In the multi-channel case it is possible to analytically find the optimal filter coefficients, provided the transform orders are given. In practice, however, an iterative method is preferred. In the multi-stage case it is not possible to find analytic solutions, so an iterative method must be used to begin with.

3.2 Optimization of Orders in the Multi-Channel Filtering Configuration

In this section, we concentrate on the multi-channel filtering case, and consider the improvement of optimizing over the M orders in addition to the filter coefficients. We first find the optimal filter coefficients for a larger number P of uniformly chosen orders and then maintain the most important ones. More specifically, we start with P uniformly chosen orders, where P is several times the number of orders M we are eventually going to use. Then the M orders resulting in filters with the highest energies are chosen, and the other $P - M$ branches of the multi-channel configuration are eliminated. Finally, with the M orders thus chosen, we reoptimize the filter coefficients. Here, we should note that the method proposed does not give the global optimum for the orders but gives the orders that provides improvements compared to uniformly choosing the orders.

As an example, we will consider the problem of synthesizing light with a desired mutual intensity. Here we wish to synthesize a system \mathbf{H} such that, when light of given mutual intensity is present at the input, light whose mutual intensity is as close as possible to the given specification is obtained at the output. Choosing to work with one-dimensional signals for simplicity, we let $f(x)$ and $g(x)$ denote the input and output optical fields, and $R_f(x_1, x_2)$ and $R_g(x_1, x_2)$ denote the input and output mutual intensities. If $f(x)$ and $g(x)$ are the input and output of a system characterized by a kernel $H(x, x')$ such that $g(x) = \int H(x, x')f(x') dx'$, then the input and output mutual intensities are related by

$$R_g(x_1, x_2) = \int \int R_f(x'_1, x'_2)H(x_1, x'_1)H^*(x_2, x'_2)dx'_1 dx'_2, \quad (3.3)$$

where H^* denotes the complex conjugate of H . The sampled, discrete version of the optical fields will be represented by column vectors \mathbf{f} and \mathbf{g} and the mutual intensity functions will be represented by matrices \mathbf{R}_f and \mathbf{R}_g . Then, we have $\mathbf{g} = \mathbf{H}\mathbf{f}$, where \mathbf{H} is the discrete form of the system kernel and the double integral relationship above assumes the following matrix form:

$$\mathbf{R}_g = \mathbf{H}\mathbf{R}_f\mathbf{H}^\dagger, \quad (3.4)$$

where \mathbf{H}^\dagger is the Hermitian conjugate of \mathbf{H} . Equation 3.4 is quadratic in \mathbf{H} . We are going to employ an equivalent representation which is linear. Since mutual intensity matrices \mathbf{R} are Hermitian and positive semi-definite, it is possible to diagonalize them as

$$\mathbf{R} = \mathbf{U}\mathbf{D}\mathbf{U}^\dagger, \quad (3.5)$$

where \mathbf{D} is a diagonal matrix whose elements are the real eigenvalues, and \mathbf{U} is a matrix whose columns constitute the set of orthonormal eigenvectors of \mathbf{R} so that $\mathbf{U}^\dagger\mathbf{U} = \mathbf{I}$, where \mathbf{I} is the identity matrix. Letting $\mathbf{D}^{1/2}$ denote the diagonal matrix whose elements are the positive square roots of the elements of \mathbf{D} , we substitute $\mathbf{D}^{1/2}\mathbf{U}^\dagger\mathbf{U}\mathbf{D}^{1/2}$ for \mathbf{D} in the above equation:

$$\mathbf{R} = \mathbf{U}\mathbf{D}^{1/2}\mathbf{U}^\dagger\mathbf{U}\mathbf{D}^{1/2}\mathbf{U}^\dagger. \quad (3.6)$$

Now, using this expansion for both \mathbf{R}_g and \mathbf{R}_f , we can write equation 3.4 as

$$\begin{aligned}\mathbf{R}_g &= \tilde{\mathbf{R}}_g \tilde{\mathbf{R}}_g^\dagger = \tilde{\mathbf{R}}_g \tilde{\mathbf{R}}_g = \tilde{\mathbf{R}}_g^2, \\ \mathbf{R}_f &= \tilde{\mathbf{R}}_f \tilde{\mathbf{R}}_f^\dagger = \tilde{\mathbf{R}}_f \tilde{\mathbf{R}}_f = \tilde{\mathbf{R}}_f^2,\end{aligned}\tag{3.7}$$

where

$$\begin{aligned}\tilde{\mathbf{R}}_g &= \tilde{\mathbf{R}}_g^\dagger = \mathbf{U} \mathbf{D}^{1/2} \mathbf{U}^\dagger \\ \tilde{\mathbf{R}}_f &= \tilde{\mathbf{R}}_f^\dagger = \mathbf{U} \mathbf{D}^{1/2} \mathbf{U}^\dagger\end{aligned}\tag{3.8}$$

Substituting 3.8 into 3.4 we obtain the following:

$$\tilde{\mathbf{R}}_g \tilde{\mathbf{R}}_g^\dagger = \mathbf{H} \tilde{\mathbf{R}}_f \tilde{\mathbf{R}}_f^\dagger \mathbf{H}^\dagger.\tag{3.9}$$

One way of satisfying the above equation is to ensure that

$$\tilde{\mathbf{R}}_g = \mathbf{H} \tilde{\mathbf{R}}_f,\tag{3.10}$$

or

$$\mathbf{H} = \tilde{\mathbf{R}}_g \tilde{\mathbf{R}}_f^{-1}.\tag{3.11}$$

In our numerical examples, we are going to consider the input light source to be incoherent. Assuming this source extends uniformly from $-r_0$ to r_0 , its mutual intensity can be written as

$$\mathbf{R}_f(x_1, x_2) = \delta(x_1 - x_2) \text{rect} \left(\frac{x_1}{2r_0} \right).\tag{3.12}$$

When discretized, the corresponding matrix \mathbf{R}_f (and its square root $\tilde{\mathbf{R}}_f$) is equal to the identity \mathbf{I} , provided r_0 is larger than the interval over which we sample. Therefore, the matrix \mathbf{H} we wish to approximate is simply equal to $\tilde{\mathbf{R}}_g$.

As a first example, we wish to synthesize a Gaussian Schell-model beam with mutual intensity:

$$R_g(x_1, x_2) = \exp \left(-\frac{(x_1 - x_2)^2}{2r_1^2} \right) \exp \left(-\frac{x_1^2 + x_2^2}{2r_2^2} \right).\tag{3.13}$$

(In our examples $r_1 = 5$ and $r_2 = 10$, in suitable units.) When we synthesize the filter \mathbf{H} corresponding to this mutual intensity using the multi-channel configuration with $M = 3$ filters ($a_1 = 1/3, a_2 = 2/3, a_3 = 1$), the normalized error turns out to be 15.42 %. Using the proposed method of optimizing the orders with $P = 12$, we find that the optimal orders are $a_1 = 2/12, a_2 = 5/12, a_3 = 10/12$, and the normalized error using these orders becomes 12.64 %. When we synthesize the same \mathbf{H} with $M = 2$ filters ($a_1 = 1/2, a_2 = 1$), the normalized error is 22.36 %. Optimizing the orders with $P = 8$, we find that the optimal orders are $a_1 = 2/8, a_2 = 6/8$, and the normalized error using these orders is 16.36 %. Further simulations have been undertaken for other values of M and P and the result errors are plotted in Figure 3.2(b). Part a of this figure shows the desired mutual intensity, part c shows the synthesized mutual intensity for $M = 2$ without optimization of orders, and part d shows the synthesized mutual intensity for $M = 2$ with optimization of orders with $P = 8$.

As a second example, we consider the synthesis, as closely as possible, of a mutual intensity profile specified as

$$R_g(x_1, x_2) = \text{rect}\left(\frac{|x_1 - x_2|}{2r_1}\right) \text{rect}\left(\frac{x_1}{2r_2}\right) \text{rect}\left(\frac{x_2}{2r_2}\right), \quad (3.14)$$

where $r_2 > r_1$. This amounts to specifying the amplitude of light at two points to be fully correlated when the distance between those points is less than $2r_1$, and totally uncorrelated otherwise. Since the rectangle function does not represent a physically realizable mutual intensity function (it is not positive semi-definite), its negative eigenvalues will be replaced by zero in obtaining its square root representation. This amounts to replacing the rectangle function with the closest positive semi-definite function. When we synthesize the filter \mathbf{H} corresponding to this mutual intensity using the multi-channel configuration with $M=3$ filters ($a_1 = 1/3, a_2 = 2/3, a_3 = 1$), the normalized error is 15.35 %. Using the proposed method of optimizing the orders with $P = 12$, we find that the optimal orders are $a_1 = 2/12, a_2 = 6/12, a_3 = 10/12$, and the normalized error using these orders is

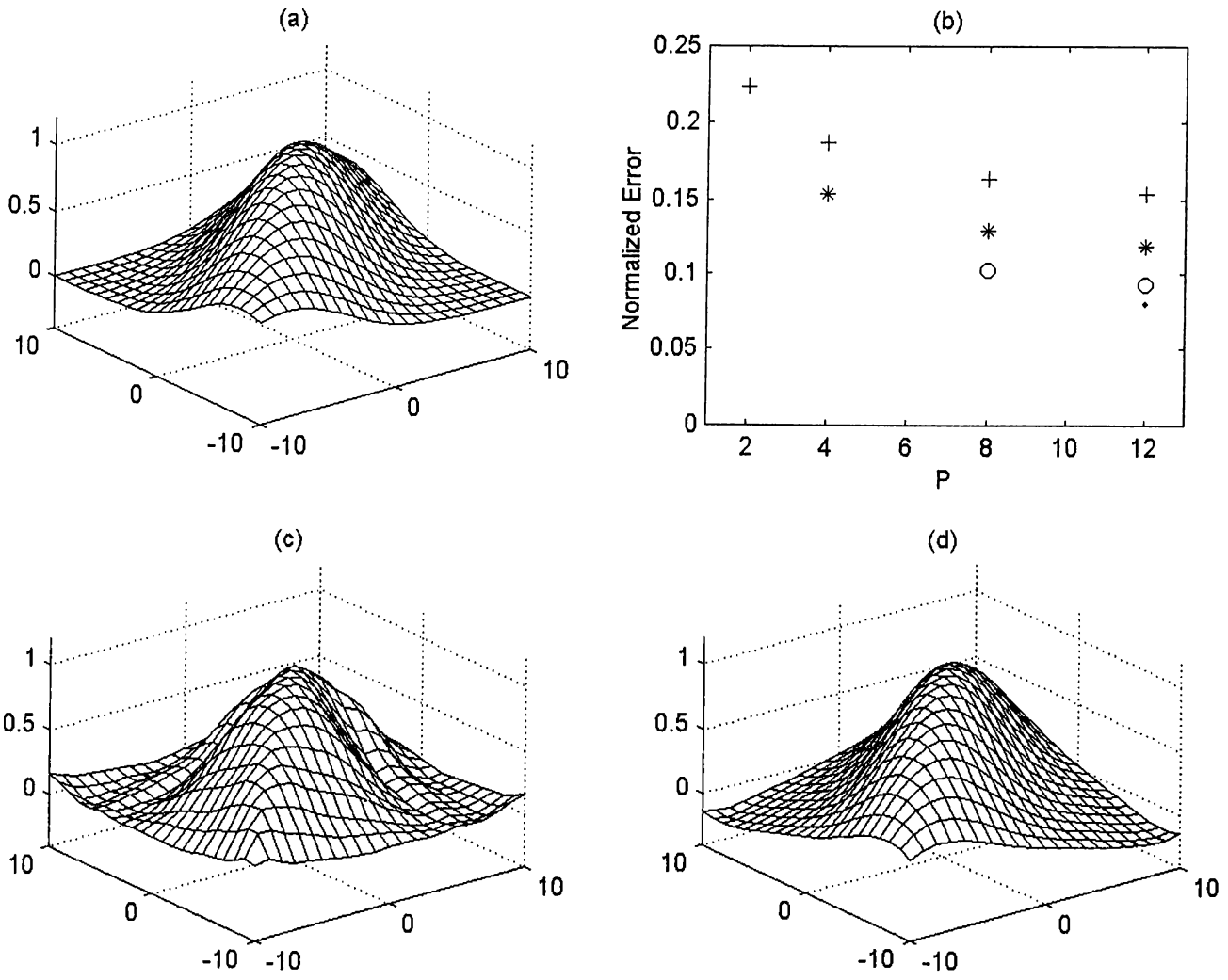


Figure 3.2: a) Desired Gaussian Schell-model mutual intensity profile. b) Normalized error vs P for different values of M ($M = 2$: '+', $M = 4$: '*', $M = 8$: 'o', $M = 12$: '.'). c) Synthesized profile using uniform orders ($M = 2$). d) Synthesized profile using optimized orders ($M = 2$, $P = 8$).

12.3 %. When we synthesize the same \mathbf{H} with $M=2$ filters ($a_1 = 1/2, a_2 = 1$), the normalized error is 22.64 %. Optimizing the orders with $P = 8$, we find that the optimal orders are $a_1 = 2/8, a_2 = 6/8$, and the normalized error using these orders is 15.45 %. Once again, further simulations have been undertaken for other values of M and P and are plotted in Figure 3.3(b). Part a of this figure shows the desired mutual intensity, part c shows the synthesized mutual intensity for $M = 2$ without optimization of orders, and part d shows the synthesized mutual intensity for $M = 2$ with optimization of orders with $P = 8$.

A number of conclusions can be drawn by examining the numerical results. First, optimization of the orders is capable of offering tangible improvements with respect to choosing the orders uniformly. We also observe that beyond a certain value of P , further increases in this parameter do not offer further reductions in the error (the benefits of optimizing over the orders is saturated). This is because further increasing P merely allows further refinements and fine-tuning in choosing the optimal orders, which has diminishing return once one moves roughly closer to the optimal orders. Also, we can see that improvements coming from optimization of the orders are greater when M is smaller but less when M is larger. This is because when M is large to begin with, it is already possible to concentrate the filtering action in those domains which are optimal. This of course means that the other domains add cost to the system implementation with little benefit, and the method we propose is useful precisely because it allows these low benefit domains to be pruned.

In conclusion, we have presented a simple and effective way of optimizing the orders in fractional Fourier domain based multi-channel filtering configurations. Until now, the orders had mostly been chosen uniformly since there was no simple way of solving the nonlinear problem of optimizing over the orders. The method we proposed is more likely to be useful when confronted with low-cost, rather than high-accuracy applications, because larger improvements are obtained when the use of a smaller number of filters is desired. Future work might include extending

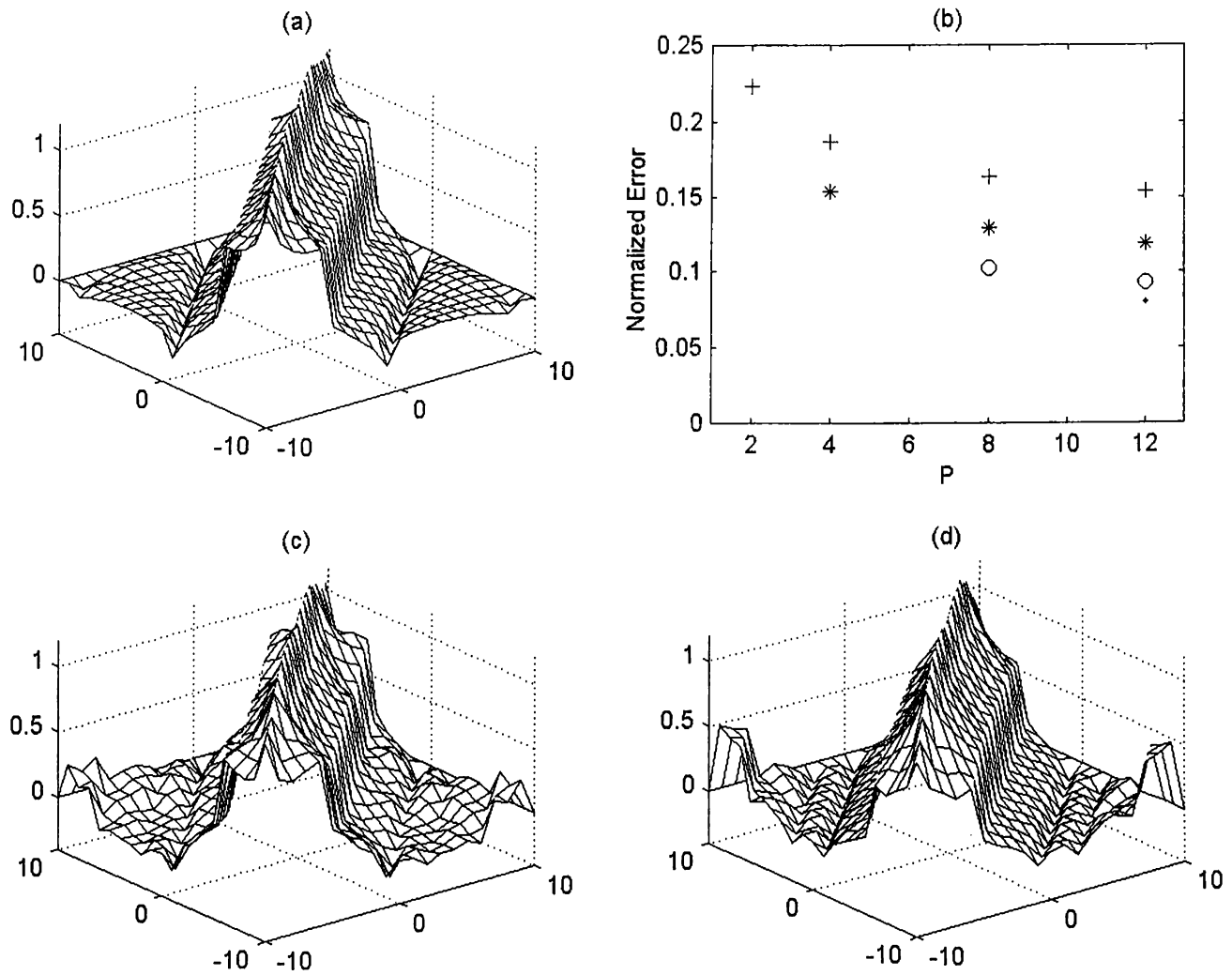


Figure 3.3: a) Desired rectangular mutual intensity profile. b) Normalized error vs P for different values of M ($M = 2$: '+', $M = 4$: '*', $M = 8$: 'o', $M = 12$: '.'). c) Synthesized profile using uniform orders ($M = 2$). d) Synthesized profile using optimized orders ($M = 2$, $P = 8$).

the method to the multi-stage case, which poses a number of challenges, and to more general filtering circuits.

Chapter 4

Image Representation and Compression with the Fractional Fourier Transform

There has been a tremendous amount of work on data compression in general and image compression [49] in particular, leading to efficient compression algorithms. In this chapter, we discuss a novel way of representing images based on fractional Fourier domain filtering configurations [47, 48], leading to an image coding method.

In Chapter 3, we have introduced the fractional Fourier transform based filtering configurations. Here, we repeat the matrices representing the overall effect of the multi-stage and multi-channel filtering configurations:

$$\mathbf{T}_{\text{ms}} = \left[\mathbf{F}^{-a_M} \mathbf{\Lambda}_{h_M} \dots \mathbf{F}^{a_2 - a_1} \mathbf{\Lambda}_{h_1} \mathbf{F}^{a_1} \right], \quad (4.1)$$

$$\mathbf{T}_{\text{mc}} = \left[\sum_{k=1}^M \mathbf{F}^{-a_k} \mathbf{\Lambda}_k \mathbf{F}^{a_k} \right] \quad (4.2)$$

In this chapter, we interpret the matrices \mathbf{T}_{mc} and \mathbf{T}_{ms} not as representing

a linear system, but as representing a two-dimensional signal or image. Thus the filtering coefficients in the multi-stage or multi-channel approximation of this matrix, can be used to approximately represent and reconstruct this matrix and the associated image. In other words, the optimal filtering coefficients minimizing the mean square error between the original matrix and its multi-stage and multi-channel approximation, are taken as the compressed version of the image. Reconstruction of compressed images is possible in $O(MN \log N)$ time. The cited work on synthesis of space-variant systems for fast implementation shows that satisfactory approximations are possible with moderate numbers of filters and hence large reductions in implementation cost. Therefore, it seems worth investigating whether similar approximations with similar reductions in cost (measured by the compression ratio) is possible when these configurations are used for image compression. Since the original image has N^2 pixels and the compressed data has NM pixels, the compression ratio is N/M .

In the multi-channel filtering case, we have also considered the improvement of optimizing over the orders as described in Chapter 3.

The compression method proposed is tested on the 128×128 image shown in Figure 4.1(a). Figure 4.1(b) shows the trade-off between the reconstruction error and compression ratio. The mean square error has been normalized by the energy of the original image. The horizontal axis of the plot is the inverse of this normalized error. We see that the multi-channel and multi-stage configurations give comparable results, though the multi-stage configuration is slightly better. Optimizing over the orders for the multi-channel case results in tangible improvements.

Figure 4.1(c,d) show illustrative results obtained with the multi-stage configuration. Although the order-optimized multi-channel case yields smaller errors, we present results for the multi-stage configuration so as to illustrate the performance of the method in its rawest, most basic form. Whereas we observe that nearly an order of magnitude compression is possible with moderate errors,

larger compression ratios are accompanied by larger errors.

Unfortunately, we observe that the use of fractional Fourier domain filtering configurations for image compression, does not yield results as good as those obtained when they are used for synthesis and fast implementation of shift-variant linear systems. In its present form, the proposed idea does not yield better results than presently available compression algorithms. However, we emphasize that the results presented reflect the performance of the basic method in its rawest and barest form; we merely represent the image with the filter coefficients which make the forms given in (3.1) and (3.2) as close as possible to the image matrix. Further refinement and development of the method and its combination and joint use with other techniques may lead to full-fledged compression algorithms with better performance. Also, it is possible to use the discrete fractional cosine transform which is a real transform, since images we are dealing with are real and a real transform would therefore reduce the cost. (One way of generalizing the method, which can lead to potentially higher compression ratios with similar errors is to employ filtering circuits based on linear canonical transforms, rather than fractional Fourier transforms [50].)

Moreover, regardless of the performance that can ultimately be obtained with improvements of the present idea, the fact that the information inherent in an image can be decomposed or factored into fractional Fourier domains in the manner described is of considerable conceptual significance. In a sense, these domains “span” a certain space which is a subset of the image space, although the precise nature of this is difficult to ascertain in the nonlinear multi-stage case. The information contained in the image is distributed to the different domains in an unequal way, making some domains more dispensable than others in representing the image. Exploring and exploiting these issues seem potentially rewarding.

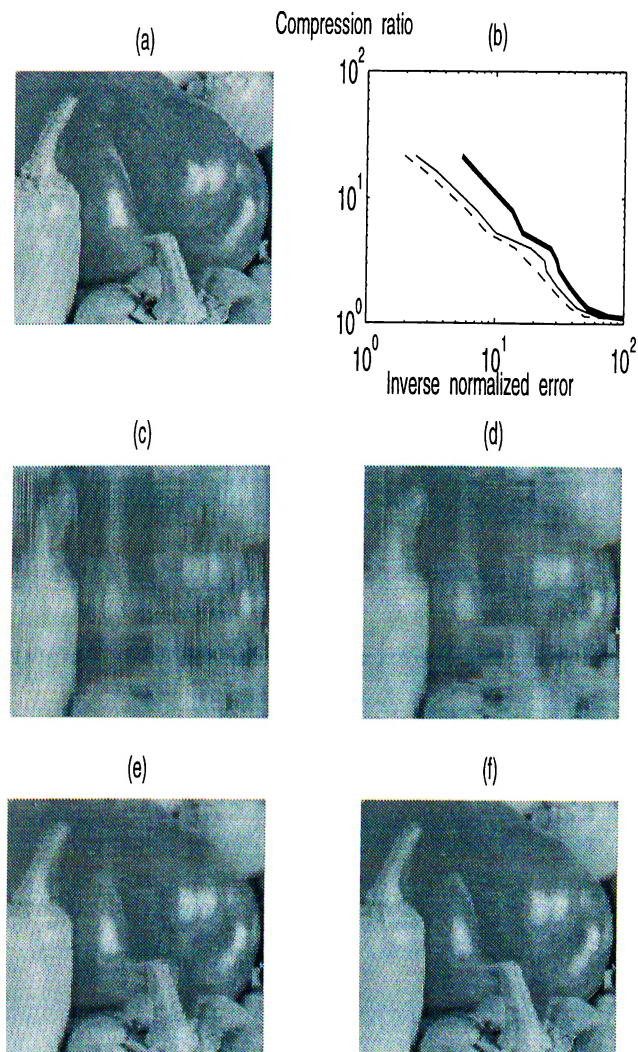


Figure 4.1: (a) Original image. (b) Compression ratio vs inverse normalized error: multi-channel (dashed line), multi-stage (solid line), multi-channel with optimized orders (bold line). Reconstructed images with compression ratio 32 (c), 21.3 (d), 8 (e), 5.3 (f). Part c and d represent too much error to be considered compressed versions of the original image. However, they have been shown to illustrate the dependence of the error on the number of coefficients used.

Chapter 5

Continuous Fractional Fourier Domain Decomposition

The continuous spectral decomposition (or expansion) and its discrete counterpart, the singular value decomposition (SVD), plays a fundamental role in signal and system analysis, representation and processing. The spectral decomposition of a function $h(u, u')$ is

$$h(u, u') = \int_{-\infty}^{\infty} \psi_v(u) \lambda_v \psi_v^*(u') dv, \quad (5.1)$$

where the λ_v are the eigenvalues and the $\psi_v(u)$ are the eigenfunctions of $h(u, u')$ (that is, they are solutions of the equation $\int_{-\infty}^{\infty} h(u, u') f(u') du' = \lambda f(u)$).

In this chapter, we define the continuous fractional Fourier domain decomposition (FFDD). While the FFDD may not match the spectral decomposition's central importance, we believe it is of fundamental importance in its own right as an alternative which may offer complementary insight and understanding. We believe the FFDD has the potential to become a useful tool in signal and system analysis, representation, and processing (especially in time-frequency space), in some cases in a similar spirit to the SVD.

Let $h(u, u')$ be a two-dimensional function, representing either an image or

the kernel of a one-dimensional linear system. Its fractional Fourier domain decomposition is defined as

$$h(u, u') = \int_{-2}^2 \int_{-\infty}^{\infty} K_{-a}(u, u'')c(a, u'')K_a(u'', u') du'' da, \quad (5.2)$$

where $c(a, u'')$ is a family of one-dimensional weighting functions with parameter a . The integration interval is limited to $[-2, 2]$, since the fractional Fourier transform is periodic in a with period 4. We can obtain $c(a, u'')$ by solving the integral equation 5.2. Sampling this equation we obtain a matrix equation which can be solved by using the tools of the linear algebra. Comparing the fractional Fourier decomposition with the spectral decomposition given in (5.1), we can see that the integrands in both expressions consist of three terms. The definition of the FFDD can be rewritten in the form

$$h(u, u') = \int_{-2}^2 \int_{-\infty}^{\infty} c(a, u'')P_a(u, u', u'') du'' da \quad (5.3)$$

where we have defined

$$P_a(u, u', u'') = K_a(u'', u')K_{-a}(u, u'') \quad (5.4)$$

Equation (5.3) can be interpreted as an expansion of $h(u, u')$ in terms of the basis functions $P_a(u', u'', u''')$ with $c(a, u'')$ corresponding to the expansion coefficients.

The basis functions in (5.4) can easily be shown to be linearly independent as a direct consequence of the fact that $\langle K_a(u'', u), K_{a'}(u, u'') \rangle_u$ is nonzero for all a, a' . Here $\langle \cdot, \cdot \rangle_u$ denotes a one-dimensional inner product with respect to the variable u .

A natural extension of the FFDD would be the linear canonical domain decomposition (LCDD) based on linear canonical transforms [50].

Chapter 6

Perspective Projections and Fractional Fourier Transforms

6.1 Introduction

Perspective projections are used in many applications in image and video processing, especially when confronted with natural or artificial scenes with depth (for instance, in robot vision applications). Perspective projections can be considered as a geometric or pointwise transformation, in the sense that each point of the object is mapped to another point in the perspective projection [51–53]. In this chapter we will examine the perspective projection in the space-frequency plane and show that its effect on the object can be modeled in terms of the fractional Fourier transform [56].

The Wigner distribution of an exponential function $\exp[i2\pi\xi x]$ is a line delta lying parallel to the space axis:

$$W_f(x, \sigma_x) = \delta(\sigma_x - \xi), \quad (6.1)$$

and the Wigner distribution of a chirp function $\exp[i\pi(\chi x^2 + 2\xi x + \zeta)]$ is an oblique line delta:

$$W_f(x, \sigma_x) = \delta(\sigma_x - \chi x - \xi). \quad (6.2)$$

To understand why the fractional Fourier transform is expected to play a role in perspective projections, let us consider the perspective projection of an image exhibiting periodic features, such as a railroad track. More “distant” parts of the image will appear in the projection smaller than “closer” parts. Thus a periodic or harmonic feature of certain frequency will be mapped such that it exhibits a monotonic increasing frequency. Under certain conditions, this increase can be assumed linear so that the harmonic function is mapped to a chirp function. Since fractional Fourier transforms are known to map harmonic functions to chirp functions, we expect that perspective projections can be modeled in terms of fractional Fourier transforms. The purpose of this chapter is to formulate this relationship.

In the next section, we are going to present the perspective model we use and examine the effect of the perspective projection on the Wigner distribution. In the following section, we will discuss the relation between the fractional Fourier transform and perspective projections based on their effects on the Wigner distribution. We will discuss how perspective projections can be modeled as shifted and fractional Fourier transformation. The last section is devoted to an analysis of the errors and the region of validity of the approximations.

6.2 Perspective Projections

The perspective model we use is shown in Figure 6.1. Initially we consider perspective projections for one-dimensional signals, since this significantly simplifies the presentation. The horizontal axis, labeled x , represents the original object space. The vertical axis, labeled x_p , represents the perspective projection space. The point A with coordinates $(-x_0, x_{p0})$ is the center of projection. We denote the original signal (object) by $f(x)$ and its perspective projection by $g(x_p)$. We assume that most of the energy of $f(x)$ is confined to the interval $[\bar{x} - \Delta x/2, \bar{x} + \Delta x/2]$. In the frequency domain, we assume that most of

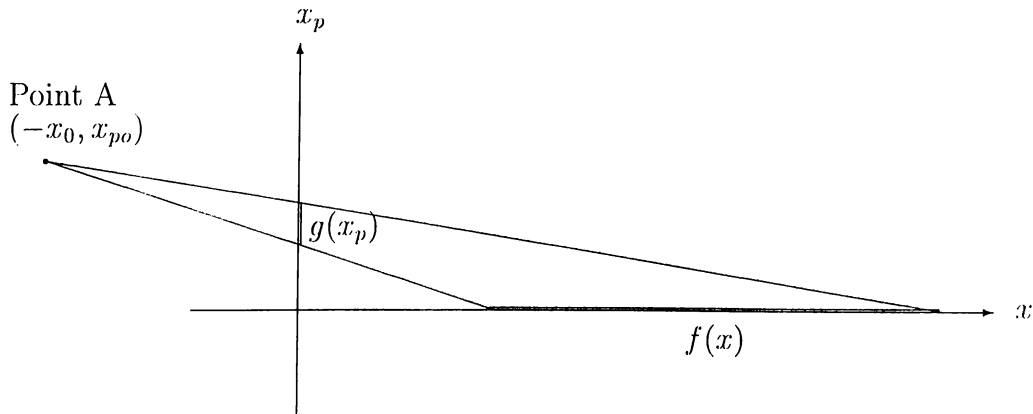


Figure 6.1: Perspective model: $f(x)$ represents the object distribution on the x axis, $g(x_p)$ represents its perspective projection onto the x_p axis. The point A with coordinates $(-x_0, x_{p0})$ is the center of projection.

the energy of $F(\sigma_x)$, the Fourier transform of $f(x)$, is confined to the interval $[\bar{\sigma}_x - \Delta\sigma_x/2, \bar{\sigma}_x + \Delta\sigma_x/2]$. The value of $f(x)$ at each x is mapped to the point x_p , which is the projection of the point x :

$$x_p = \frac{x x_{p0}}{x + x_0}, \quad (6.3)$$

$$x = \frac{x_0 x_p}{x_{p0} - x_p}, \quad (6.4)$$

which can be derived by simple geometry. Thus, the projection $g(x_p)$ is expressed as follows:

$$g(x_p) = f\left(\frac{x_0 x_p}{x_{p0} - x_p}\right). \quad (6.5)$$

The interval to which most of the energy of $g(x_p)$ is approximately confined can be determined using (6.3).

In order to see the effect of perspective projections in the space-frequency plane, we decompose $f(x)$ into harmonics as follows:

$$f(x) = \int F(\sigma_x) \exp(i2\pi x \sigma_x) d\sigma_x. \quad (6.6)$$

where $F(\sigma_x)$ is the Fourier transform of $f(x)$. Using (6.5) and linearity we obtain

the following expression for $g(x_p)$:

$$g(x_p) = \int F(\sigma_x) h(x_p, \sigma_x) d\sigma_x, \quad (6.7)$$

where

$$h(x_p, \sigma_x) = \exp \left[i2\pi\sigma_x \left(\frac{x_0 x_p}{x_{po} - x_p} \right) \right] d\sigma_x. \quad (6.8)$$

We will initially concentrate on a single exponential with frequency $\bar{\sigma}_x$ and study the effect of perspective projection in the space-frequency plane. Then, we will construct $g(x_p)$ by first decomposing $f(x)$ in terms of exponentials and using (6.7).

The Wigner distribution of $h(x_p, \bar{\sigma}_x)$ cannot be explicitly obtained. Therefore, to continue our analytical development, we expand the phase of $h(x_p, \bar{\sigma}_x)$ in a Taylor series. We will expand the phase of $h(x_p, \bar{\sigma}_x)$ around the point which \bar{x} is mapped to:

$$\frac{\bar{x}}{\bar{x} + x_0} x_{po} \quad (6.9)$$

which we express as κx_{po} where $\kappa = \frac{\bar{x}}{\bar{x} + x_0}$. Expanding the phase of $h(x_p, \bar{\sigma}_x)$ around κx_{po} we obtain the following after some algebra:

$$h(x_p, \bar{\sigma}_x) = \exp \left[i2\pi\sigma_x x_0 \left(\frac{x_p^2}{(1 - \kappa)^3 x_{po}^2} + \frac{x_p(1 - 3\kappa)}{(1 - \kappa)^3 x_{po}} + \frac{\kappa^3}{(1 - \kappa)^3} + \dots \right) \right]. \quad (6.10)$$

Ignoring terms higher than the second order, the projection of a harmonic is seen to be a chirp function. The validity of this approximation requires the third order term to be much smaller than the second order term:

$$|\kappa + 2| \ll |2x_{po}(\kappa - 1)|. \quad (6.11)$$

This approximation is more accurate for larger values of x_{po} . This is expected since larger x_{po} correspond to less deep perspective projections. The Wigner distribution of the chirp given in (6.10) is a line delta given by:

$$\delta \left[\sigma_x + \frac{2\bar{\sigma}_x}{(1 - \kappa)^3 x_{po}^2} x_p + \frac{\bar{\sigma}_x(1 - 3\kappa)}{(1 - \kappa)^3 x_{po}} \right], \quad (6.12)$$

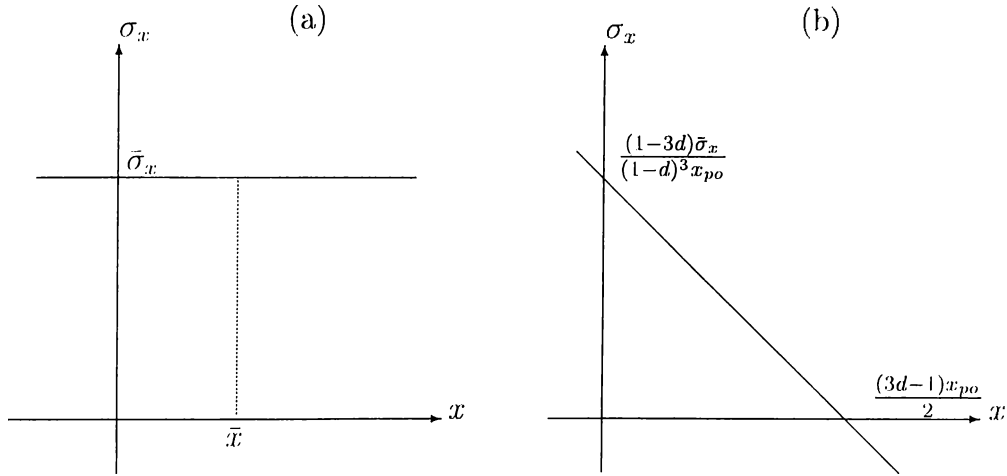


Figure 6.2: (a) Wigner distribution of the original exponential. (b) Wigner distribution of the approximate perspective projection: a chirp.

and is shown in Figure 6.2b.

Having obtained an approximate analytical form for the perspective projection of a harmonic, as well as its Wigner distribution, we now move on to our discussion of perspective projections in the space-frequency plane, as well as its relation to the fractional Fourier transform.

6.3 Perspective Projections and Fractional Fourier Transforms

In the previous section, we obtained an approximate expression for the Wigner distribution of the perspective projection of a single exponential. The Wigner distribution of a typical exponential and the Wigner distribution of the approximate perspective projection of the exponential are shown in Figure 6.2. The angle the line delta makes with the x axis is $\arctan \left[\frac{2\bar{\sigma}_x}{(1-\kappa)^3 x_{p0}^2} \right]$, which depends on $\bar{\sigma}_x$. The fact that the oblique line delta is a rotated version of the horizontal line delta suggests a role for the fractional Fourier transform since this operation

corresponds to rotation in the space-frequency plane.

We will now show how the perspective projection of a signal can be approximately expressed in terms of the fractional Fourier transform. We claim that the perspective projection of a signal can be obtained from, or modeled by, the following steps:

1. Shift the signal by \bar{x} in the negative x direction and by $\bar{\sigma}_x$ in the negative σ_x direction. This translates the Wigner distribution of the signal to the origin of the space-frequency plane.
2. Take the fractional Fourier transform with the order $a = \frac{-2}{\pi} \arctan \left[\frac{2\bar{\sigma}_x(\bar{x}+x_0)^3}{x_{po}^2 x_0^2} \right]$. This rotates the Wigner distribution by an angle $a\pi/2$.
3. Shift the result by $\frac{\bar{x}x_{po}}{\bar{x}+x_0}$ in the positive x direction and by $\frac{\bar{\sigma}_x(\bar{x}+x_0)^2}{x_0 x_{po}}$ in the positive σ_x direction.

These steps represent a decomposition of the overall effect of the perspective projection, from which we see that the substance of perspective projection is essentially to effect a rotation in the space-frequency plane. However, this rotation is enacted on the space-frequency content of the signal referred to the origin of the space-frequency plane. The above steps are illustrated in Figure 6.3.

Different frequency components of the signal require different fractional Fourier orders, because the order a given in step 3 depends on $\bar{\sigma}_x$. However, as we will see, under certain conditions, a satisfactory approximation can be obtained by using a uniform order corresponding to the central frequency of the signal.

We now demonstrate our claim that perspective projection can be decomposed into the three steps given above. We start by decomposing $f(x)$ into harmonics:

$$f(x) = \int F(\sigma_x) \exp(2i\pi x\sigma_x) d\sigma_x, \quad (6.13)$$

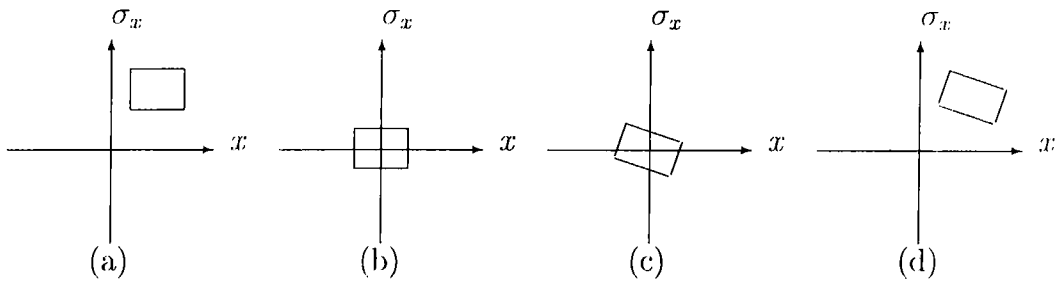


Figure 6.3: Illustration of the decomposition of the approximation into elementary operations in the space-frequency plane. a) Original signal. b) After step 1 (Space and frequency shift). c) After step 2 (Fractional Fourier transform.) d) After step 3 (Space and frequency shift): Approximate perspective projection.

We will concentrate on a single harmonic component $\exp(i2\pi x\sigma_x)$ and the result for general $f(x)$ will follow by linearity. Applying step 1 to a single harmonic we obtain

$$\exp(i2\pi\bar{x}\sigma_x). \quad (6.14)$$

Now, we apply step 2 and step 3 to this result to obtain

$$\left(1 + i\frac{2\sigma_x\bar{x} + x_0}{x_{po}^2x_0^3}\right)^{1/2} \exp(i2\pi\bar{x}\sigma_x) \exp\left[\left(i2\pi x^2\sigma_x\frac{\bar{x} + x_0}{x_{po}^2x_0^3}\right)\right] \quad (6.15)$$

Finally, we apply step 4 and obtain our final result:

$$\left(1 + i\frac{2\sigma_x(\bar{x} + x_0)^3}{x_{po}^2x_0^3}\right)^{1/2} \exp(i2\pi\bar{x}\sigma_x) \exp\left[i2\pi\sigma_x\left(x - \frac{\bar{x}x_{po}}{\bar{x} + x_0}\right)^2\left(\frac{\bar{x} + x_0}{x_{po}^2x_0^3}\right)\right] \\ \times \exp\left[i4\pi\sigma_x\left(\frac{\bar{x} + x_0^2}{x_0^2x_{po}}\right)\right] \quad (6.16)$$

Multiplying this with $F(\sigma_x)$ and integrating over σ_x yields the desired approximate expression for the perspective projection of $f(x)$, which is the mathematical expression of the four steps outlined above.

To see that this expression is indeed an approximation of the perspective projection, we again concentrate on a single harmonic component whose exact perspective projection is

$$\exp\left(2i\pi\sigma_x\frac{x_0x_p}{x_{po} - x_p}\right) \quad (6.17)$$

Using the Taylor series expansion we obtain

$$\exp \left\{ i2\pi\sigma_x x_0 \left[\frac{x_p^2}{(1-\kappa)^3 x_{po}^2} + \frac{x_p(1-3\kappa)}{(1-\kappa)^3 x_{po}} + \frac{\kappa^3}{(1-\kappa)^3} \right] \right\}, \quad (6.18)$$

which differs from (6.16) only by a constant factor. As far as a single harmonic component is concerned, the only approximation that is involved is the binomial expansion in the exponent. When the harmonic components are superposed to obtain the original function $f(x)$, we make the additional approximation of using the order corresponding to the center frequency for all harmonic components. Thus our three-step procedure will deviate from the exact perspective projection more and more as the bandwidth of $f(x)$ is increased. The limitations associated with this approximation will be discussed in the next section.

Figure 6.4 shows the exact perspective projection of the function

$$\cos(4\pi x) \text{rect} \left(\frac{x-4}{6} \right) = \left[\frac{\exp(i4\pi x) + \exp(-i4\pi x)}{2} \right] \text{rect} \left(\frac{x-4}{6} \right) \quad (6.19)$$

superimposed with the approximation given by (6.18). We chose $x_0 = -3$, $x_{po} = 6$ as the center of projection. As a second example, we consider the narrowband signal shown in Figure 6.5. Again, the exact perspective projection and the fractional Fourier approximation are superimposed in part b of the same figure. We observe that the approximation is quite satisfactory except very near the edges, which should be avoided.

Generalization of the proposed method to two dimensions is possible by following similar steps. In our two-dimensional perspective model we use a two-dimensional image with midpoints \bar{x} , \bar{y} ; center frequencies $\bar{\sigma}_x$, $\bar{\sigma}_y$ and spatial widths Δx , Δy . Our center of projection is located at $(x_0, x_{po}, 0)$. The model described is shown in Figure 6.6.

With this model, using simple geometry we can obtain the following mappings and reverse mappings for each x_p and y_p :

$$x_p = \frac{x x_{po}}{x + x_0} \quad (6.20)$$

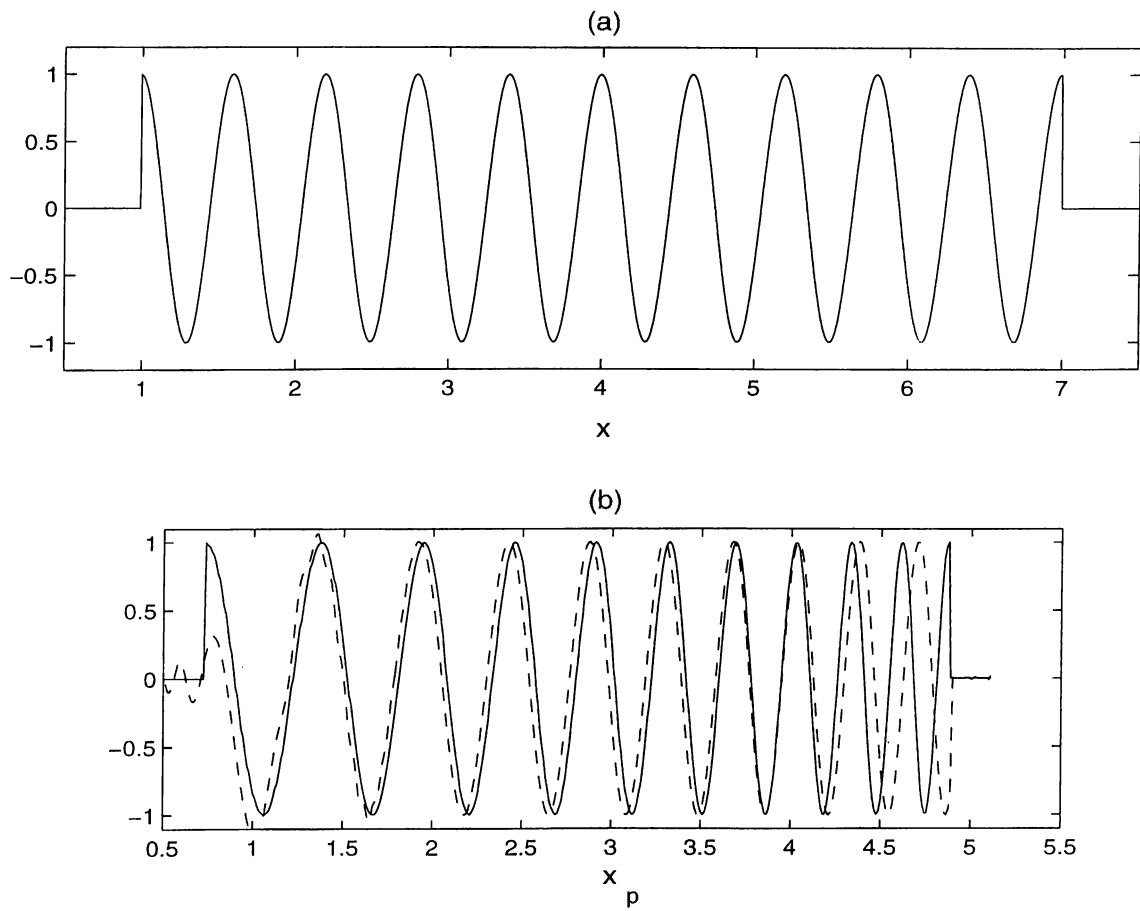


Figure 6.4: a) Original signal. b) Exact perspective projection (solid line) superimposed with the fractional Fourier approximation (dashed line).

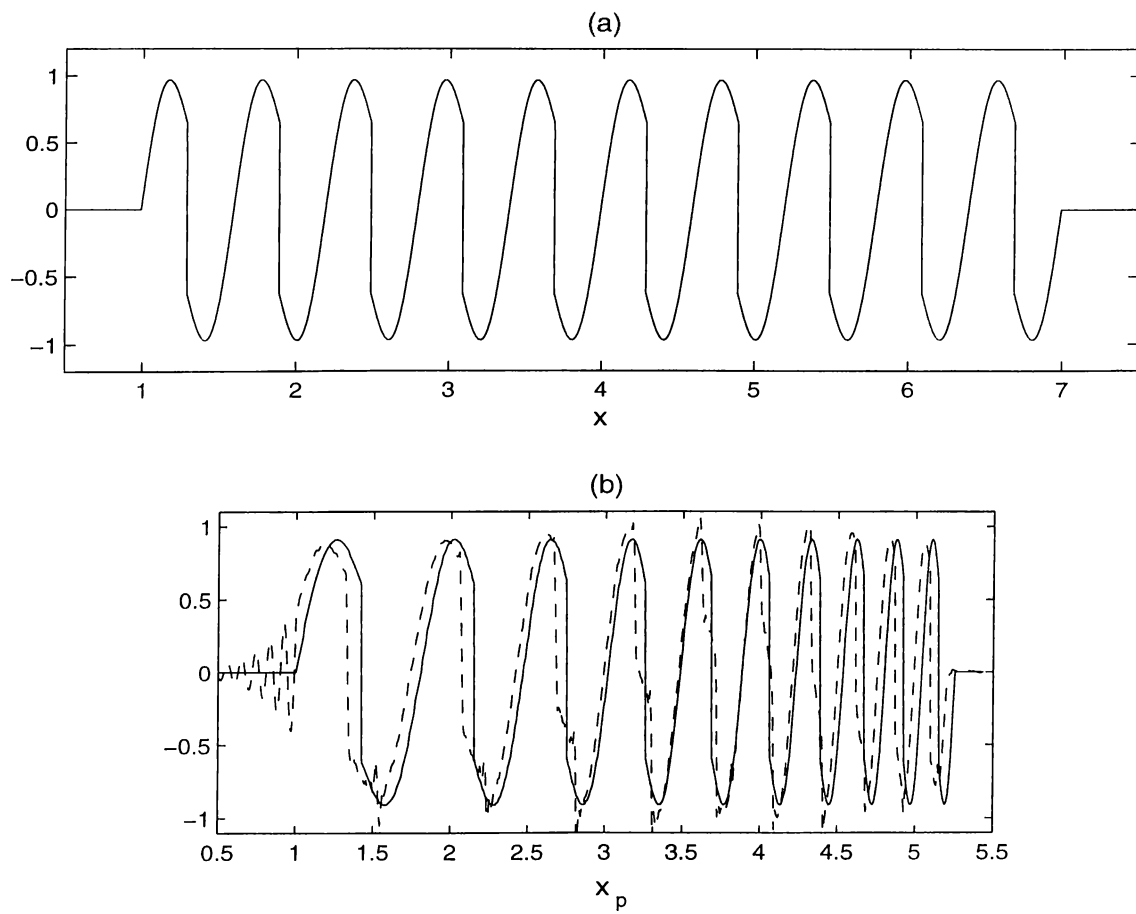


Figure 6.5: a) Original signal. b) Exact perspective projection (solid line) superimposed with the fractional Fourier approximation (dashed line).

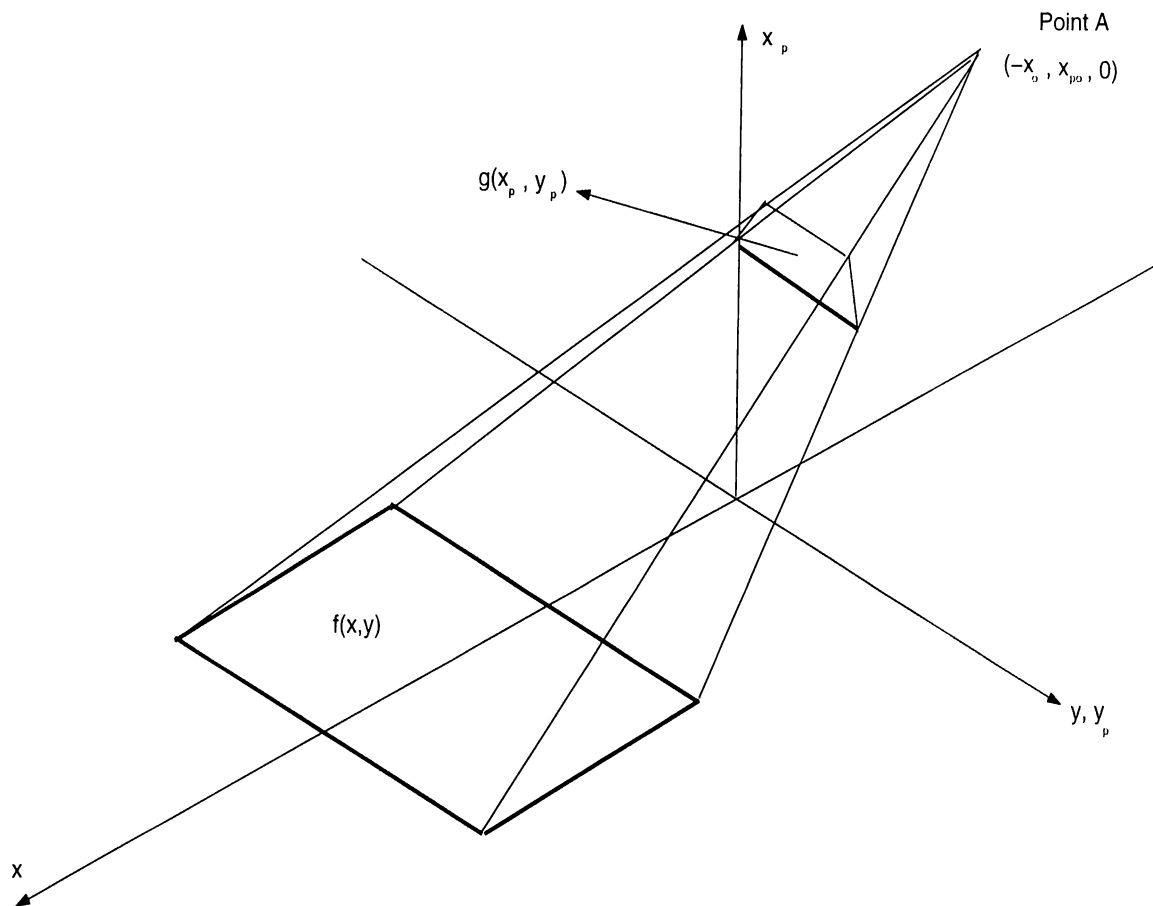


Figure 6.6: Perspective model: $f(x, y)$ represents the object distribution on the x - y plane, $g(x_p, y_p)$ represents its perspective projection onto the x_p - y_p plane. The point A with coordinates $(-x_0, x_{p0}, 0)$ is the center of projection.

$$x = \frac{x_0 x_p}{x_{p0} - x_p} \quad (6.21)$$

$$y_p = \frac{x \Delta y + 2x_0 y}{2(x + x_0)} \quad (6.22)$$

$$y = \frac{y_p x_{p0}}{x_{p0} - x_p} - \frac{x_p \Delta y}{2(x_0 - x_p)} \quad (6.23)$$

As in the one-dimensional case we first decompose $f(x, y)$ into harmonics,

$$f(x, y) = \int F(\sigma_x, \sigma_y) \exp(i2\pi\sigma_x x) \exp(i2\pi\sigma_y y) d\sigma_x d\sigma_y. \quad (6.24)$$

We proceed by writing an expression for the perspective projection of a two-dimensional harmonic $\exp[i2\pi\bar{\sigma}_x x] \exp[i2\pi\bar{\sigma}_y y]$:

$$\begin{aligned} & \exp \left[i2\pi\bar{\sigma}_x x_0 \left(\frac{x_p^2}{(1-\kappa)^3 x_{p0}^2} + \frac{x_p(1-3\kappa)}{(1-\kappa)^3 x_{p0}} + \frac{\kappa^3}{(1-\kappa)^3} \right) \right] \\ & \times \exp \left[-i\pi\bar{\sigma}_y \Delta y \left(\frac{x_p^2}{(1-\kappa')^3 x_0^2} + \frac{x_p(1-3\kappa')}{(1-\kappa')^3 x_0} + \frac{\kappa'^3}{(1-\kappa')^3} \right) \right] \\ & \times \exp \left[i2\pi\bar{\sigma}_y y_p \left(\frac{x_p^2}{x_{p0}^2 (1-\kappa)^3} + \frac{x_p(1-3\kappa)}{x_p(1-\kappa)^3} + \frac{3\kappa^2 - 3\kappa + 1}{(\kappa-1)^3} \right) \right], \end{aligned} \quad (6.25)$$

where again the binomial approximation has been employed and $\kappa = \frac{\bar{x}}{\bar{x}+x_0}$ and $\kappa' = \frac{\bar{x}}{\bar{x}+\Delta y}$. Close examination of (6.25) reveals that we have the product of a one-dimensional chirp in the x_p direction and a scaled harmonic in the y_p direction whose scaling factor depends on x_p . We are going to approximate the perspective projection by using one-dimensional shifts and one-dimensional fractional Fourier transforms followed by scaling. We claim that the two-dimensional perspective projection of a signal can be obtained from, or modeled by, the following steps:

1. Shift the signal by \bar{x} in the negative x direction and by $\bar{\sigma}_x$ in the negative σ_x direction. This translates the Wigner distribution of the signal to the origin of the space-frequency plane.
2. Take the one-dimensional fractional Fourier transforms in the variable x with order $a = \frac{-2}{\pi} \arctan \left[\frac{2\bar{\sigma}_x(\bar{x}+x_0)^3}{x_{p0}^2 x_0^2} - \frac{(\bar{x}+\Delta y)^3 \bar{\sigma}_y}{\Delta y^2 x_0^2} \right]$, treating y as a parameter. This rotates the Wigner distributions by an angle $a\pi/2$.

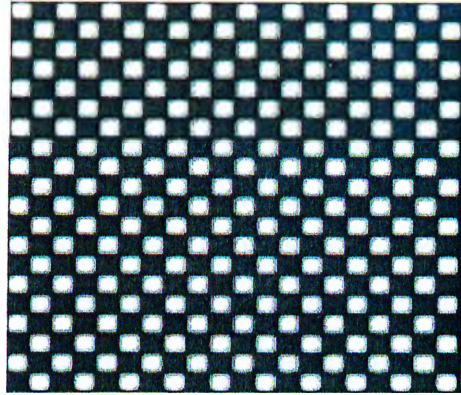
3. Shift the result by $\frac{\bar{x}x_{p0}}{\bar{x}+x_0}$ in the positive x direction and by $\left[\frac{\bar{\sigma}_x(\bar{x}+x_0)^3}{x_{p0}x_0} - \frac{(\bar{x}+\Delta y)^3\bar{\sigma}_y}{\Delta y^2x_0^2} \right]$ in the positive σ_x direction.
4. Scale each horizontal line of the perspective projection by $\left[\bar{\sigma}_y \left(\frac{x_p^2}{x_{p0}^2(1-\kappa)^3} + \frac{x_p(1-3\kappa)}{x_p(1-\kappa)^3} + \frac{3\kappa^2-3\kappa+1}{(\kappa-1)^3} \right) \right]$.

The mathematical combination of the above steps yields the two-dimensional perspective projection of a two-dimensional harmonic, given by equation (6.25). Multiplying this with $F(\sigma_x, \sigma_y)$ and integrating over σ_x and σ_y yields the desired approximate expression for the perspective projection of $f(x, y)$, which is the mathematical expression of the four steps outlined above. An example is given in Figure 6.7, where the fractional Fourier transform-based result shown in part c is seen to be a reasonable approximation of the actual perspective projection shown in part b.

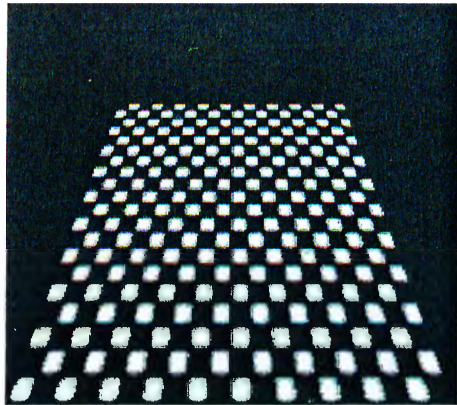
6.4 Error Analysis

In this section, we examine the conditions under which the fractional Fourier transform approximation to the perspective projection is valid. We first examine the modifications the Wigner distribution undergoes corresponding to the approximation. Since we know that the approximation can be decomposed into the four steps given in Section 6.3, it is an easy matter to find the resulting changes in the Wigner distribution. To estimate the error inherent in our approximation, we will think of the original Wigner distribution as consisting of horizontal strips of narrow frequency components. The major approximation we make is to replace the fractional orders required by these different frequency components by a single order corresponding to the central frequency. To determine the error introduced by this approximation, we will determine how the highest and lowest frequency strips would be mapped had their individual frequencies been used instead of the center frequency. Let us assume that most of the energy of the Wigner

(a)



(b)



(c)

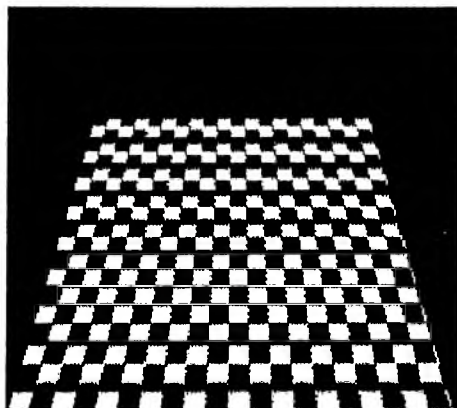


Figure 6.7: a) Original signal. b) Exact perspective projection. c) Fractional Fourier approximation.

distribution of a signal is concentrated in a rectangular region in the space-frequency plane (Figure 6.8a). Part b of the same figure shows the Wigner distribution corresponding to the fractional Fourier approximation (solid lines). The dashed lines, on the other hand, show the Wigner contour obtained by using the individual frequencies for the highest and lowest frequency strips.

Our error criteria will be the deviations of the corners of the two superimposed Wigner contours in Figure 6.8b. There will be one spatial deviation and one frequency deviation for each of the four corners of the contours. We will normalize the spatial deviation by Δx and the frequency deviations by $\Delta\sigma_x$ and take the maximum of the resulting eight normalized deviations as our final error measure. Expression for the eight normalized deviations are given below:

$$\begin{aligned}
e_{\text{up-left,space}} &= \frac{\Delta\sigma_x}{\Delta x x_0} \sin\left(\frac{\alpha_c - \alpha_u}{2}\right) \left[\cos\left(\frac{\alpha_c + \alpha_u}{2}\right) + \frac{1}{x_0} \sin\left(\frac{\alpha_c + \alpha_u}{2}\right) \right], \\
e_{\text{up-right,space}} &= \frac{\Delta\sigma_x}{\Delta x x_0} \sin\left(\frac{\alpha_c - \alpha_u}{2}\right) \left[\cos\left(\frac{\alpha_c + \alpha_u}{2}\right) - \frac{1}{x_0} \sin\left(\frac{\alpha_c + \alpha_u}{2}\right) \right], \\
e_{\text{low-left,space}} &= -\frac{\Delta\sigma_x}{\Delta x x_0} \sin\left(\frac{\alpha_c - \alpha_d}{2}\right) \left[\cos\left(\frac{\alpha_c + \alpha_d}{2}\right) + \frac{1}{x_0} \sin\left(\frac{\alpha_c + \alpha_d}{2}\right) \right], \\
e_{\text{low-right,space}} &= -\frac{\Delta\sigma_x}{\Delta x x_0} \sin\left(\frac{\alpha_c - \alpha_d}{2}\right) \left[\cos\left(\frac{\alpha_c + \alpha_d}{2}\right) - \frac{1}{x_0} \sin\left(\frac{\alpha_c + \alpha_d}{2}\right) \right], \\
e_{\text{up-left,freq.}} &= -\frac{1}{x_0} \sin\left(\frac{\alpha_c - \alpha_u}{2}\right) \left[\sin\left(\frac{\alpha_c + \alpha_u}{2}\right) + \frac{\Delta x}{\Delta\sigma_x x_0} \cos\left(\frac{\alpha_c + \alpha_u}{2}\right) \right], \\
e_{\text{up-right,freq.}} &= -\frac{1}{x_0} \sin\left(\frac{\alpha_c - \alpha_u}{2}\right) \left[\sin\left(\frac{\alpha_c + \alpha_u}{2}\right) - \frac{\Delta x}{\Delta\sigma_x x_0} \cos\left(\frac{\alpha_c + \alpha_u}{2}\right) \right], \\
e_{\text{low-left,freq.}} &= \frac{1}{x_0} \sin\left(\frac{\alpha_c - \alpha_d}{2}\right) \left[\sin\left(\frac{\alpha_c + \alpha_d}{2}\right) + \frac{\Delta x}{\Delta\sigma_x x_0} \cos\left(\frac{\alpha_c + \alpha_d}{2}\right) \right], \\
e_{\text{low-right,freq.}} &= \frac{1}{x_0} \sin\left(\frac{\alpha_c - \alpha_d}{2}\right) \left[\sin\left(\frac{\alpha_c + \alpha_d}{2}\right) - \frac{\Delta x}{\Delta\sigma_x x_0} \cos\left(\frac{\alpha_c + \alpha_d}{2}\right) \right],
\end{aligned}$$

where

$$\alpha_c = \arctan\left[\frac{2\frac{\sigma_x}{x_0}\left(\frac{x+x_0}{x_0}\right)^3}{\left(\frac{x p_0}{x_0}\right)^2}\right], \quad \alpha_u = \arctan\left[\frac{2\left(\frac{\sigma_x}{x_0} + \frac{\Delta\sigma_x}{2x_0}\right)\left(\frac{x+x_0}{x_0}\right)^3}{\left(\frac{x p_0}{x_0}\right)^2}\right]$$

and

$$\alpha_d = \arctan\left[\frac{2\left(\frac{\sigma_x}{x_0} - \frac{\Delta\sigma_x}{2x_0}\right)\left(\frac{x+x_0}{x_0}\right)^3}{\left(\frac{x p_0}{x_0}\right)^2}\right]$$

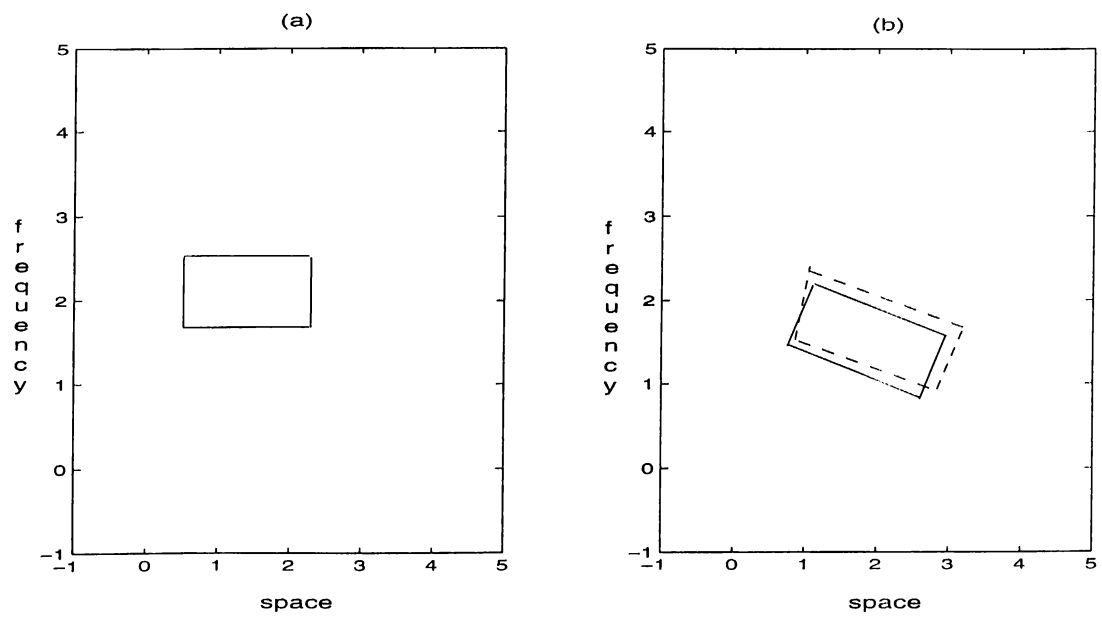


Figure 6.8: (a) Wigner distribution of the original signal. (b) Comparison of Wigner distributions underlying error analysis.

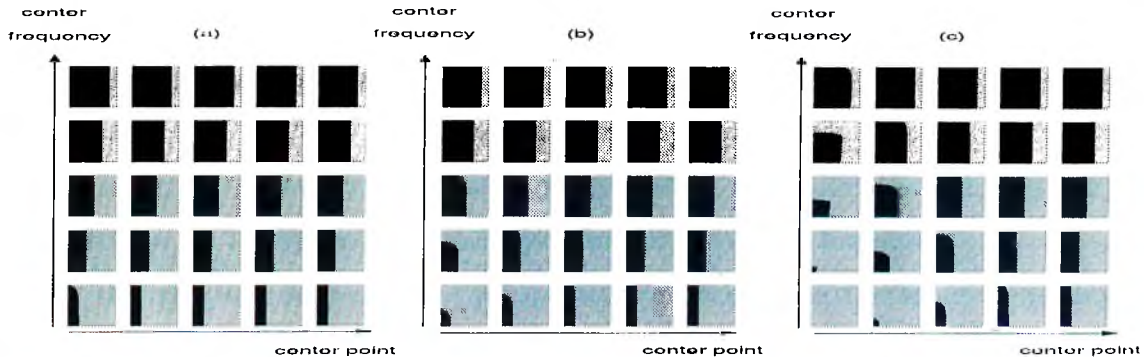


Figure 6.9: The dark regions represent the parameter combinations whose normalized error is less than 10%. See text for explanation.

To reduce the number of parameters by one, we have expressed the above results so that all free parameters appear divided by x_0 .

It does not seem possible to analytically derive conclusions using these formulae so that we will resort to numerically obtained plots. The approximation will be assumed to be acceptable if the maximum normalized error is less than 10%. The above given expressions give the error as a function of six variables: $x_0, x_{po}, \bar{x}, \bar{\sigma}_x, \Delta x, \Delta \sigma_x$. However, normalizing all variables by x_0 , the number of variables can be reduced to five. Figure 6.9 shows the region where the maximum normalized error is less than 10% as darker regions, whereas the lighter regions are where the error is large. The horizontal axis in each of the 75 plots represents the value of $\Delta x/x_0$ and the vertical axis represents $\Delta \sigma_x/x_0$. Both of these variables range from $10^{1/30}$ to $10^{100/30}$ in these log-log plots.

Each member of the 5×5 matrices of plots corresponds to different values of \bar{x}/x_0 (horizontal) $\bar{\sigma}_x/x_0$ (vertical). The five separate values of \bar{x}/x_0 are $10^{-1/2}, 10^{0/2}, 10^{1/2}, 10^{2/2}, 10^{3/2}$ and the five separate values of $\bar{\sigma}_x/x_0$ are $10^{-1/2}, 10^{0/2}, 10^{1/2}, 10^{2/2}, 10^{3/2}$. The three groups of 25 plots each correspond to different values of the center of projection. Figure 6.9a: $x_{po}/x_0 = 0.1$, Figure 6.9b: $x_{po}/x_0 = 1$, Figure 6.9c: $x_{po}/x_0 = 10$.

This set of plots covering a broad range of the parameter values allows us to determine whether the approximation developed is acceptable for a certain range of parameters. Generally speaking, we have larger acceptable regions for larger values of $\bar{\sigma}_x$. Not surprisingly, the approximation is strained as Δx and $\Delta\sigma_x$ increase, i.e. as the space-bandwidth product of the signal increases.

In this chapter, we examined perspective projections in the space-frequency plane and showed how to approximate the perspective projection in terms of the fractional Fourier transform. Our main motivation was that the fractional Fourier transform approximately captures the essence of the warping characteristic of perspective projections. We observed that perspective projection approximately maps harmonic components into chirps and therefore can be modeled in terms of the fractional Fourier transform. We saw that the substance of perspective projection is essentially to effect a rotation in the space-frequency plane. However, this rotation is enacted on the space-frequency content of the signal referred to the origin of the space-frequency plane. Elementary numerical examples for both one-dimensional signals and two-dimensional images are presented. The errors associated with the approximation and the region of validity with respect to the approximations involved are numerically discussed. In natural scenes, it is more typical to encounter periodic or nearly periodic patterns as opposed to chirp-like patterns. If such assumptions can be quantified and posed into a form of constraints, then it may be possible to estimate the transform order and center of projection associated with a perspective image and recover the original undistorted image.

Chapter 7

Conclusions and Future Work

The fractional Fourier transform is a generalization of the ordinary Fourier transform and therefore supersedes the ordinary Fourier transform. With the extra parameter that the fractional Fourier transform provides, any application where ordinary Fourier transform is used, is a potential application area where the fractional Fourier transform can yield improvements. In this thesis, we have illustrated some of these applications.

In Chapter 3, we have presented a simple and effective way of optimizing the orders in fractional Fourier domain based multi-channel filtering configurations. Until now, the orders had mostly been chosen uniformly since there was no simple way of solving the nonlinear problem of optimizing over the orders. The method we proposed is more likely to be useful when confronted with low-cost, rather than high-accuracy applications, because larger improvements are obtained when the use of a smaller number of filters is desired. Future work might include extending the method to the multi-stage case, which poses a number of challenges, and to more general filtering circuits. Also, another interesting direction of research is the selection of filtering configurations for a given specific application.

We have used the fractional Fourier transform based filtering configurations in image representation and compression in Chapter 4. In its present form, the

proposed idea does not yield better results than presently available compression algorithms. However, we emphasize that the results presented reflect the performance of the basic method in its rawest and barest form. The information contained in the image is distributed to the different domains in an unequal way, making some domains more dispensable than others in representing the image. Exploring and exploiting these issues seem potentially rewarding. Further refinement and development of the method and its combination and joint use with other techniques may lead to full-fledged compression algorithms with better performance. (One way of generalizing the method, which can lead to potentially higher compression ratios with similar errors is to employ filtering circuits based on linear canonical transforms, rather than fractional Fourier transforms [50].)

A chapter is devoted to the continuous fractional Fourier domain decomposition. A future work would be the linear canonical domain decomposition (LCDD) based on linear canonical transforms [50].

In Chapter 6, we have examined perspective projections in the space-frequency plane and showed how to approximate the perspective projection in terms of the fractional Fourier transform. Our main motivation was that the fractional Fourier transform approximately captures the essence of the warping characteristic of perspective projections. We observed that perspective projection approximately maps harmonic components into chirps and therefore can be modeled in terms of the fractional Fourier transform. We saw that the substance of perspective projection is essentially to effect a rotation in the space-frequency plane. Elementary numerical examples for both one-dimensional signals and two-dimensional images are presented. The errors associated with the approximation and the region of validity with respect to the approximations involved are numerically discussed.

Future work in this area might include the extension of the analysis to wide-band signals by using multiple orders. Another promising direction is to optimize over the single order used in approximating the narrow-band signals' perspective projections rather than simply using the order corresponding to the central frequency.

Some part of this thesis was previously presented. Optimization of orders which is explained in Chapter 3 is presented in [54]. Image representation and compression introduced in Chapter 4 can be found in [55]. Continuous fractional Fourier transform is previously presented in [25] and analysis of perspective projections in the space-frequency plane is published previously in [56].

Bibliography

- [1] A. V. Oppenheim and R. W. Schaffer. *Digital Signal Processing*, Prentice-Hall, New Jersey, 1989
- [2] H. M. Ozaktas, M. A. Kutay and Z. Zalevsky. *The Fractional Fourier Transform with Applications in Optics and Signal Processing*. John Wiley and Sons, 2000.
- [3] N. Wiener. Hermitian polynomials and Fourier analysis. *J. Math. Phys. MIT*, 18:70-73, 1929.
- [4] E. U. Condon. Immersion of the Fourier transform in a continuous group of functional transformations. *Proc. Natl. Acad. Sci. USA*, 23:158-164, 1937.
- [5] V. Bargmann. On a Hilbert space of analytic functions and an associated integral transform, Part I. *Comm. Pure Appl. Math.*, 14:187-214, 1961.
- [6] V. Namias. The fractional order Fourier transform and its application to quantum mechanics. *J. Inst. Math. Appl.*, 25:241-265, 1980.
- [7] D. A. Mustard. Uncertainty principles invariant under the fractional Fourier transform. *J. Aus. Math. Soc. B*, 33:180-191, 1991.
- [8] B. Yurke, W. Schleich and D. F. Walls. Quantum superpositions generated by quantum nondemolition measurements. *Phys. Rev. A.*, 42:1703-1711, 1990.

- [9] H. M. Ozaktas and D. Mendlovic, Fractional Fourier optics, *J. Opt. Soc. Am. A*, 12:743 – 751, 1995.
- [10] S. Abe and J. T. Sheridan. Comment on ‘The fractional Fourier transform in optical propagation problems.’ *J. Mod. Opt.*, 42:2373–2378, 1995.
- [11] T. Alieva and F. Agullo-Lopez. Diffraction analysis of random fractal fields. *J. Opt. Soc. Am. A*, 15:669–674, 1998.
- [12] W. X. Cong, N. X. Chen and B. Y. Gu. Beam shaping and its solution with the use of an optimization method. *Appl. Opt.*, 37:4500–4503, 1998.
- [13] R. G. Dorsch and A. W. Lohmann. Fractional Fourier transform used for a lens design problem. *Appl. Opt.*, 34:4111–4112, 1995.
- [14] D. Dragoman and M. Dragoman. Near and far field optical beam characterization using the fractional Fourier transform. *Opt. Comm.*, 141:5–9, 1997.
- [15] S. Granieri, O. Trabocchi and E. E. Sicre. Fractional Fourier transform applied to spatial filtering in the Fresnel domain. *Opt. Comm.*, 119:275–278, 1995.
- [16] A. W. Lohmann, D. Mendlovic and Z. Zalevsky. Fractional transformations in optics. In *Progress in Optics XXXVIII*, Elsevier, Amsterdam, 1998. Chapter IV, pages 263–342.
- [17] H. M. Ozaktas and O. Aytür. Fractional Fourier domains. *Sig. Proc.*, 46:119–124, 1995.
- [18] M. A. Kutay, H. M. Ozaktas, O. Arikan and L. Onural. Optimal filtering in fractional Fourier domains. *IEEE Trans. Sig. Proc.*, 45:1129–1143, 1997.
- [19] M. A. Kutay and H. M. Ozaktas. Optimal image restoration with the fractional Fourier transform. *J. Opt. Soc. Am. A*, 15:825–833, 1998.

- [20] M. F. Erden, M. A. Kutay and H. M. Ozaktas. Repeated filtering in consecutive fractional Fourier domains and its application to signal restoration. *IEEE Trans. Sig. Proc.*, 47:1458–1462, 1999.
- [21] M. F. Erden and H. M. Ozaktas. Synthesis of general linear systems with repeated filtering in consecutive fractional Fourier domains. *J. Opt. Soc. Am. A*, 15:1647–1657.
- [22] M. F. Erden, H. M. Ozaktas and D. Mendlovic. Synthesis of mutual intensity distributions using the fractional Fourier transform. *Opt. Comm.*, 125:288–301, 1996.
- [23] M. A. Kutay. Generalized filtering configurations with applications in digital and optical signal and image processing. PhD Thesis. *Bilkent Univ., Dept. of Electrical and Electronics Eng.*, 1996.
- [24] M. A. Kutay, H. Özaktaş, H. M. Ozaktas and O. Arikan. Fractional Fourier Domain Decomposition, *Sig. Proc.*, 77:105–109, 1999.
- [25] İ. Ş. Yetik, M. A. Kutay, H. Özaktaş and H. M. Ozaktas. Continuous and Discrete Fractional Fourier Domain Decomposition. In *Proceedings of the 2000 IEEE International Conference on Acoustics, Speech, and Signal Processing*, pages I:93–96. IEEE, Piscataway, New Jersey, 2000.
- [26] H. M. Ozaktas and D. Mendlovic. Fourier transforms of fractional order and their optical interpretation. *Opt. Comm.*, 101:163–169, 1993.
- [27] D. Mendlovic, H. M. Ozaktas and A. W. Lohmann. Fractional Correlation. *Appl. Opt.*, 34:303–309, 1995.
- [28] A. W. Lohmann, Z. Zalevsky and D. Mendlovic. Synthesis of pattern recognition filters for fractional Fourier processing. *Opt. Comm.*, 128:199–204, 1996.

- [29] Z. Zalevsky, I. Raveh, G. Shabtay, D. Mendlovic and J. Garcia. Single output color pattern recognition using a fractional correlator. *Opt. Eng.*, 36:2127–2136, 1997.
- [30] O. Guleryuz. Feature extraction with the fractional Fourier transform. M. S. Thesis. *Bilkent Univ., Dept. of Electrical and Electronics Eng.*, 1998.
- [31] C. J. Kuo and Y. Luo. Generalized joint fractional Fourier transform correlators: a compact approach. *Appl. Opt.*, 37:8270–8276, 1998.
- [32] D. Mendlovic, Z. Zalevsky, A. W. Lohmann and R. G. Dorsch. Signal spatial-filtering using the localized fractional Fourier transform. *Opt. Comm.*, 126:14–18, 1996.
- [33] Z. Zalevsky and D. Mendlovic. Fractional Wiener filter. *Appl. Opt.*, 35:3930–3936, 1996.
- [34] Z. Zalevsky, D. Mendlovic and J. H. Caulfield. Localized, partially space-invariant filtering. *Appl. Opt.*, 36:1086–1092, 1997.
- [35] T. Alieva. Fractional Fourier transform as a tool for investigation of fractal objects. *J. Opt. Soc. Am. A*, 13:1189–1192, 1996.
- [36] L. M. Bernardo and O. D. D. Soares. Fractional Fourier transforms and imaging. *J. Opt. Soc. Am. A*, 11:2622–2626, 1994. 35:297–303, 1996.
- [37] J. García, D. Mendlovic, Z. Zalevsky and A. Lohmann. Space-variant simultaneous detection of several objects by the use of multiple anamorphic fractional-Fourier-transform filters. *Appl. Opt.*, 35:3945–3952, 1996.
- [38] L. B. Almeida, The fractional Fourier transform and time-frequency representations, *IEEE Trans. Sig. Proc.*, 42:3084–3092, 1994.
- [39] S. C. Pei and M. H. Yeh, Improved discrete fractional Fourier transform, *Opt. Lett.*, 22:1047–1049, 1995.

- [40] L. B. Almeida. The fractional Fourier transform and time-frequency representations. *IEEE Trans. Sig. Proc.* 42:3084–3092, 1994.
- [41] O. Akay and G. F. Boudreaux-Bartels. Unitary and Hermitian fractional operators and their relation to the fractional Fourier transform. *IEEE Sig. Proc. Lett.*, 5:312–314, 1998.
- [42] L. Cohen. *Time-Frequency Analysis*. Prentice Hall PTR, Englewood Cliffs, New Jersey, 1995.
- [43] H. M. Ozaktas, O. Arıkan, M. A. Kutay and G. Bozdađı. Digital computation of the fractional Fourier transform. *IEEE Trans. Sig. Proc.*, 44:2141–2150, 1996.
- [44] C. Candan, M. A. Kutay and H. M. Ozaktas The Discrete Fractional Fourier Transform. *IEEE Trans. Sig. Proc.*, 48:1329–1337, 2000.
- [45] A. Sahin. Two-dimensional fractional Fourier transform and its optical implementation. M.S. Thesis. *Bilkent Univ., Dept. of Electrical and Electronics Eng.*, 1996.
- [46] H. M. Ozaktas, B. Barshan, D. Mendlovic, and L. Onural. Convolution, filtering, and multiplexing in fractional Fourier domains and their relation to chirp and wavelet transforms. *J. Opt. Soc. Am. A* 11:547–559, 1994.
- [47] M. A. Kutay, M. F. Erden, H. M. Ozaktas, O. Arıkan, Ö. Güleryüz, and Ç. Candan. Space-Bandwidth Efficient Realizations of Linear Systems, *Opt. Lett.*, 23:1069–1071, 1998.
- [48] H. M. Ozaktas, M. A. Kutay, and D. Mendlovic. Introduction to the fractional Fourier transform and its applications. In Peter W. Hawkes, editor, *Advances in Imaging and Electron Physics, Volume 106*, pages 239–291. Academic Press, San Diego, California, 1999.

- [49] A. K. Jain. *Fundamentals of Digital Image Processing*. Prentice-Hall, New Jersey, 1989.
- [50] B. Barshan, M. A. Kutay, and H. M. Ozaktas, Optimal filtering with linear canonical transforms, *Opt. Comm.*, 135:32–36,1997.
- [51] D. Vernon. *Machine vision: Automated Visual Inspection and Robot Vision*. Prentice Hall New York, 1991.
- [52] A. Low. *Introductory Computer Vision and Image Processing*. McGraw-Hill New York, 1991.
- [53] G. Woldberg. *Digital Image Warping*. IEEE Comp. Soc. Press Los Alamitos, CA, 1992.
- [54] İ. Ş. Yetik, M. A. Kutay, and H. M. Ozaktas. Optimization of Orders in Multi-Channel Fractional Fourier Domain Filtering Circuits and Its Application to the Synthesis of Mutual Intensity Distributions, to be submitted.
- [55] İ. Ş. Yetik, M. A. Kutay, and H. M. Ozaktas. Image representation and compression with the fractional Fourier transform , to be submitted.
- [56] İ. Ş. Yetik, H. M. Ozaktas, B. Barshan and L. Onural. Perspective Projections in the Space-Frequency Plane and Fractional Fourier Transforms. *J. Opt. Soc. Am. A*, Vol. 17, 2000.